

NPS ARCHIVE  
1962  
KINLEY, F.

A SPECTROSCOPIC INVESTIGATION OF  
AN ARGON GLOW DISCHARGE

FREDERIC H. M. KINLEY,  
and  
ROBERT J. O'MALIA

LIBRARY  
U.S. NAVAL POSTGRADUATE SCHOOL  
MONTEREY, CALIFORNIA









A SPECTROSCOPIC INVESTIGATION OF AN

ARGON GLOW DISCHARGE

\* \* \* \* \*

Frederic H.M. Kinley

and

Robert J. O'Malia





A SPECTROSCOPIC INVESTIGATION OF AN  
ARGON GLOW DISCHARGE

by

Frederic H.M. Kinley  
Lieutenant, United States Navy

and

Robert J. O'Malia  
Lieutenant, United States Navy

Submitted in partial fulfillment of  
the requirements for the degree of

MASTER OF SCIENCE  
IN  
PHYSICS

United States Naval Postgraduate School  
Monterey, California

1962

NPS Archive  
1962

~~Thesis~~  
~~K46~~

Kinley, F.

A SPECTROSCOPIC INVESTIGATION OF AN

ARGON GLOW DISCHARGE

by

Frederic H.M. Kinley

and

Robert J. O'Malia

This work is accepted as fulfilling  
the thesis requirements for the degree of

MASTER OF SCIENCE

IN

PHYSICS

from the

United States Naval Postgraduate School



## ABSTRACT

The visible spectrum from argon glow discharges was observed by means of a three-meter concave-grating spectrograph. The discharges were operated under various conditions: with moving striations in the positive column and without striations, and in the presence and absence of a helical instability. The principal results are as follows. No argon ion spectrum was observed at any position in the tube. No changes in the spectrum from the positive column were observed with changing operating conditions. Electrode materials were observed as impurities in the discharge near the electrodes.

The helical instability was induced by a longitudinal magnetic field. An investigation of the critical field, which was required to initiate the instability, as a function of tube current, tube diameter and gas pressure, indicated that the critical field was sensitive to changes in all three parameters and to the transition of the discharge from the striated to the striation-free condition.

A study of the feasibility of detection of a Doppler shift revealed that the longitudinal velocity of radiating atoms could be detected by crossing a Fabry-Perot interferometer with a prism spectrograph if the atom velocity was equal to or greater than the observed striation velocities.

The authors wish to express their gratitude to Dr. Raymond L. Kelly for his guidance, encouragement and skillfull assistance throughout their project. They would also like to express their appreciation to Dr. Alfred W. Cooper for his cooperation and advice. The assistance of the Physics Department technicians is also acknowledged.



## TABLE OF CONTENTS

Section	Title	Page
1.	Introduction	1
	1.1. The Low Pressure Gas Discharge and Moving Striations	
	1.2. The Helical Instability, Moving Striations and Critical Magnetic Field	
2.	General Features of Discharge Tube and Vacuum System	4
	2.1. Discharge Tubes and Electrodes	
	2.2. Power Supplies	
	2.3. Vacuum System	
3.	Spectrographic Observations	12
	3.1. Spectrograph and Associated Optical Equipment	
	3.2. Photographic Plate Analysis	
	3.3. Spectroscopic Procedures and Results	
4.	Helical Instability and Critical Magnetic Field	23
	4.1. Operating Procedures	
	4.2. Results and Discussion	
5.	Feasibility of Doppler Shift Measurement	32
	5.1. Theoretical Considerations	
	5.2. Interferometer and Spectrograph Arrangement	
	5.3. Tube Description	
6.	Conclusions	39
	6.1. Conclusions	
	6.2. Recommendations	
	References	41
	Appendix	43
	Identified Wavelengths	





## LIST OF ILLUSTRATIONS

Figure	Title	Page
1.	Sketch of discharge tube and electrode/filament configuration.	5
2.	Basic electronic circuit for discharge operation.	6
3.	Characteristic curve for tube DT-2.	9
4.	Characteristic curve for tube DT-3.	10
5.	Schematic diagram of vacuum system.	11
6.	Spectrograph/discharge tube orientation.	13
7.	Example of discharge spectra.	17
8.	Grotrian diagram of A I.	19
9.	Grotrian diagram of A II.	20
10.	Argon spectrum of various discharge conditions.	22
11.	Discharge tube and magnetic coil orientation (side view).	24
12.	Discharge tube and magnetic coil orientation (end view).	25
13.	Critical field vs tube current for DT-2.	26
14.	Critical field vs tube current for DT-3.	27
15.	Critical field vs gas pressure for DT-2.	29
16.	Critical field vs gas pressure for DT-3.	30
17.	Critical field vs gas pressure (comparison).	31
18.	Optical arrangement for interferometer-spectrograph combination--external method.	35
19.	Optical arrangement for interferometer-spectrograph combination--internal method (two variations).	35
20.	Tube construction.	37



## 1. INTRODUCTION

### 1.1. THE LOW PRESSURE GAS DISCHARGE AND MOVING STRIATIONS

The phenomenon of the glow discharge at low pressure, that is, pressures less than about 10 mm Hg, is well known in physics and has been studied extensively for more than a century. Brown<sup>1</sup>, Francis<sup>2</sup> and Emeleus<sup>3</sup> give complete discussions of the characteristics of the low pressure glow discharge including theories and experimental results. Moving striations, which are alternating bands of darkness and luminosity travelling through the positive column of a glow discharge, are a very little understood phenomenon although they, too, have been known for over a century. Numerous experiments have been carried out and many theories proposed in an attempt to explain moving striations but to date no completely satisfactory explanation has resulted. Pupp<sup>4</sup>, Donahue and Dieke<sup>5</sup>, Robertson<sup>6</sup>, and Pekarek<sup>7</sup>, to name but a few, have attacked the mysteries of moving striations with a variety of approaches in recent years. The use of spectroscopic methods as a diagnostic tool in the investigation of moving striations has received little attention in comparison with other devices such as rotating mirrors, probes, photomultiplier tubes and oscilloscopes. The experiments described here were undertaken to provide some basic spectroscopic information concerning moving striations as a part of the continuing research in glow discharge being conducted at the U.S. Naval Postgraduate School by Professors A. W. Cooper, R. L. Kelly and N. L. Oleson.

Because it is believed that the role of metastable states is an important one in the phenomenon of moving striations<sup>5,6</sup>, the visible spectrum of a discharge in argon, which possesses metastable states, was investigated under striated and striation-free conditions.

Initially a step-tube was used; the emitted radiation being viewed from the different sections of the tube under conditions where the small diameter center section was striation-free while at the same time the large-diameter end sections contained moving striations. Cooper<sup>8</sup> has previously investigated the conditions of current, gas pressure and tube dimensions wherein the moving striations could be preferentially established in a step-tube. Using the same step-tube, a spectroscopic analysis



of the anode and cathode regions was undertaken to determine what impurities were cast into the discharge from the electrodes and how far into the discharge these impurities penetrated.

The step-tube was replaced in later work by a straight tube for three reasons, namely, to eliminate the corner obstructions, to facilitate tube construction, and to eliminate the deposition of material at the step-section. A longitudinal magnetic field was applied to the straight tube in an attempt to concentrate a section of the discharge beam. Instead of the expected constriction of the beam, a helical instability was observed and investigated.

## 1.2. THE HELICAL INSTABILITY, MOVING STRIATIONS AND CRITICAL MAGNETIC FIELD

The observed instability occurred in the vicinity of the magnetic field solenoid coils for fields greater than a certain critical value. When the striations were present, they were observed to be moving through the helical instability as well as the rest of the discharge. Therefore, a spectroscopic investigation was made of the positive column between the solenoid coils as described in section 3.3. Using two straight tubes of different radii, an investigation was made of the critical magnetic field as a function of the tube current and argon gas pressure, with the results shown in section 4.

The helical instability was encountered by Hoh and Lehnert<sup>9</sup> during studies of particle and energy losses in the positive column of a discharge tube under the influence of a longitudinal magnetic field. Recently, Hoh<sup>10</sup> and Kadomtsev and Nadospasov<sup>11</sup> have considered the origin of the instability from two different standpoints. Hoh made use of a criterion for the stability of a wall sheath and showed that it is no longer satisfied when the magnetic field exceeds a critical value. The manner in which the failure of the sheath-stability criterion affects the discharge was not discussed. Kadomtsev and Nadospasov, on the other hand, show that perturbations of the discharge column can grow when diffusion to the walls can no longer overcome the effects of  $\vec{J} \times \vec{B}$  forces that tend to increase the perturbation. The value of critical field obtained does not depend on the magnitude of the current density. In addition to predicting the critical field, their theory predicts the frequency, wavelength



and growth rate of the oscillation. Allen, Paulikas and Pyle<sup>12</sup> have compared their experimental results with these two theories using H<sub>2</sub>, D<sub>2</sub>, He, Ne and A, in discharge tubes 250 cm long and radii of 1.27 and 0.90 cm which were placed at the axis of a solenoid which could be adjusted in length up to 200 cm.

An attempt has been made to correlate the results included here with the above two theories.







## 2. GENERAL FEATURES OF DISCHARGE TUBE AND VACUUM SYSTEM

### 2.1. DISCHARGE TUBES AND ELECTRODES

The discharge tubes used in these investigations were fabricated from pyrex tubing with an approximate wall thickness of 2 mm. Fig. 1 displays the tubes which were used, together with their dimensions and electrode/filament configuration. The nickel electrodes and tungsten filaments used were hand made at the USNPS Physics Shop, except for the filament of tube DT-1 which was commercially manufactured, and were spot-welded to the lead-in wires of a glass VG1A ionization gauge tube which in turn served as the discharge tube end. Due to the high currents, 0.5 amp to 1.1 amp, passed through the tubes during observations, the useful operating life of each tube depended upon the durability of the filaments. In order to be able to use either end of each tube as a cathode, the filaments were nearly identical. Several filament configurations were tested. The common failure of each filament was the development of a hot spot at the cathode due to ion bombardment followed by melting and separation of the wire at this spot. To reduce filament heating the hot-cathode operation was used. This method of operation requires external filament heating and provides neutralizing electrons to reduce ion bombardment; however, there was not enough electron emission to eliminate hot spot formation. In some instances the initial hot spot appeared shortly after the tube was ignited for the first time while in other instances the hot spot developed only after several hours of operation, not necessarily continuous. The best filament arrangement was that pictured for tube DT 3 in Fig. 1 for which five hours of tube operation per end was realized.

### 2.2. POWER SUPPLIES

The operation of the discharge tube required, at most, three power supplies: one for the main tube power supply, one for external filament heating and one for the Pupp's auxiliary discharge<sup>13</sup>. The basic electronic circuit used is pictured schematically in Fig. 2, and the circuit elements are listed in Table 1.



## 2. GENERAL FEATURES OF DISCHARGE TUBE AND VACUUM SYSTEM

### 2.1. DISCHARGE TUBES AND ELECTRODES

The discharge tubes used in these investigations were fabricated from pyrex tubing with an approximate wall thickness of 2 mm. Fig. 1 displays the tubes which were used, together with their dimensions and electrode/filament configuration. The nickel electrodes and tungsten filaments used were hand made at the USNPS Physics Shop, except for the filament of tube DT-1 which was commercially manufactured, and were spot-welded to the lead-in wires of a glass VG1A ionization gauge tube which in turn served as the discharge tube end. Due to the high currents, 0.5 amp to 1.1 amp, passed through the tubes during observations, the useful operating life of each tube depended upon the durability of the filaments. In order to be able to use either end of each tube as a cathode, the filaments were nearly identical. Several filament configurations were tested. The common failure of each filament was the development of a hot spot at the cathode due to ion bombardment followed by melting and separation of the wire at this spot. To reduce filament heating the hot-cathode operation was used. This method of operation requires external filament heating and provides neutralizing electrons to reduce ion bombardment; however, there was not enough electron emission to eliminate hot spot formation. In some instances the initial hot spot appeared shortly after the tube was ignited for the first time while in other instances the hot spot developed only after several hours of operation, not necessarily continuous. The best filament arrangement was that pictured for tube DT-3 in Fig. 1 for which five hours of tube operation per end was realized.

### 2.2. POWER SUPPLIES

The operation of the discharge tube required, at most, three power supplies: one for the main tube power supply, one for external filament heating and one for the Pupp's auxiliary discharge<sup>13</sup>. The basic electronic circuit used is pictured schematically in Fig. 2, and the circuit elements are listed in Table 1.



Tube number	Tube Dimensions	Electrode/Filament Arrangement	
		3 Dimensional View	Description
DT-1	<p>64.7 cm 17.7 cm 1.45 cm 5.9 cm</p>	<p>half section 2.54 cm 2.54 cm</p>	<p>Electrode: hollow cylinder</p> <p>Filament: conic spiral</p>
DT-2	<p>78.6 cm 3.8 cm</p>	<p>2.54 cm 2.54 cm</p>	<p>Electrode: hollow cylinder</p> <p>Filament: circular tightly-wound spiral (outside electrode)</p>
DT-3	<p>73.6 cm 4.5 cm</p>	<p>2.54 cm 2.54 cm</p>	<p>Electrode: hollow cylinder</p> <p>Filament: plane spiral</p>

NOTE: Filament material — tungsten; Electrode material — nickel

Fig. 1. Sketch of discharge tube and electrode/filament arrangement.



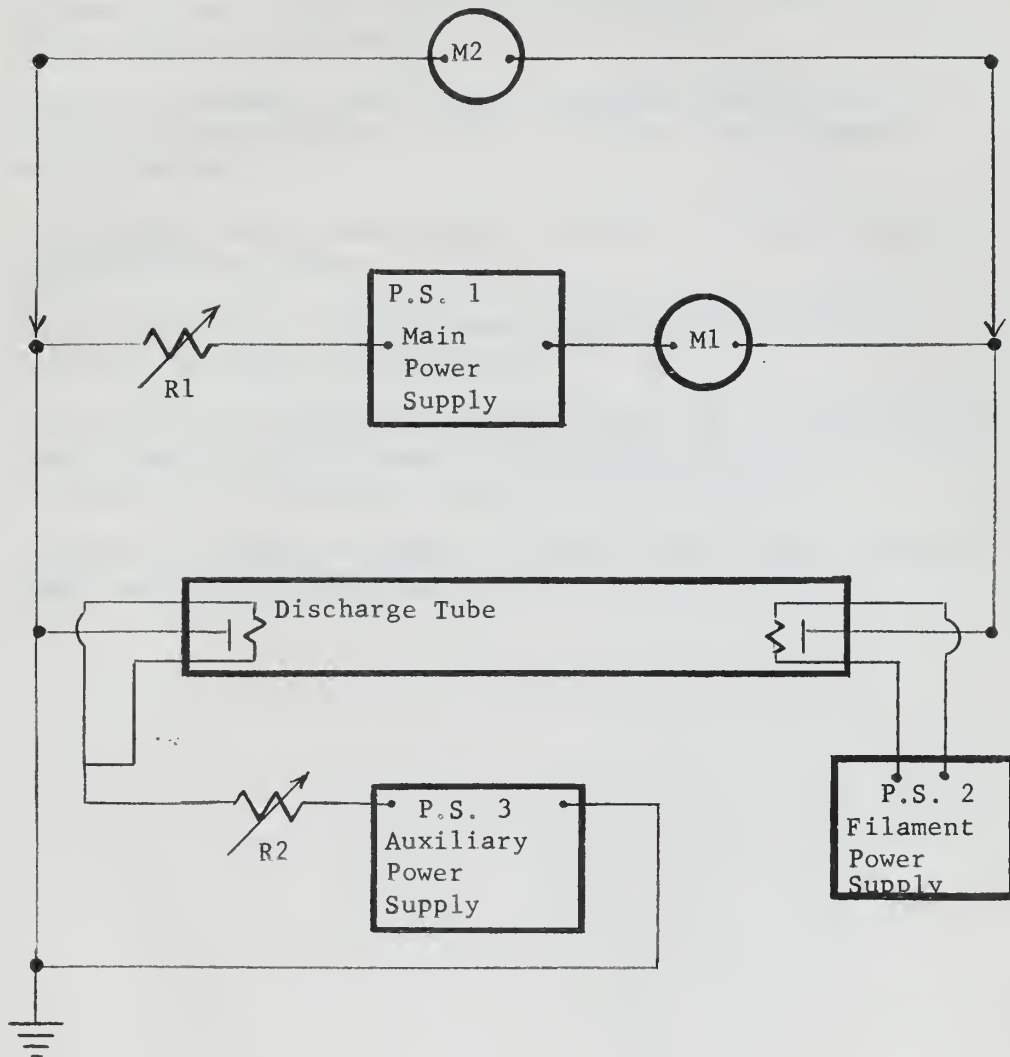


Fig. 2. Basic electronic circuit for discharge operation.







TABLE I

List of electronic components

- PS-1 Main discharge power supply; KEPCO Model 770B, 0-3.0a, 0-50v (with ammeter and voltmeter).
- PS-2 Filament power supply; KEPCO Model KM236-15a, 0-15a, 0-50v (with ammeter and voltmeter).
- PS-3 Auxiliary discharge power supply; Sorenson and Co., Inc., Model 1000-VB-NOBATRON, 0.750 ma, 0-1200v. (with ammeter and voltmeter).
- M-1 Tube current meter; Westinghouse Type PX-5, 0-1 amp, internal resistance=0.05 ohms.
- M-2 Tube voltage meter, Westinghouse Type PX-5, 0-150 volts, internal resistance= 30,000 ohms.
- R-1 Main discharge variable resistance, eight (8) Hardwich-Mindle Inc., Type C-100; 200 ohms, 1.5a, 100 watts each, (four (4) in series and in parallel with four (4) in series).
- R-2 Auxiliary discharge variable resistance; J.G. Biddle Company, 3500 ohms, 0.3a slide wire.



The externally heated filament furnished neutralizing electrons and stabilized the discharge. The Pupp's auxiliary discharge eliminated the anode spots which can occur in a gaseous discharge<sup>14</sup>. Only with tube DT-3 were the external heating and auxiliary discharge utilized simultaneously to maintain a stable discharge.

Representative characteristic curves for tubes DT-2 and DT-3 are displayed in Figures 3 and 4, respectively. The curves are comparable to those obtained from other tubes operating at similar pressures and currents<sup>13</sup>.

### 2.3. VACUUM SYSTEM

The vacuum system pictured schematically in Fig. 5 was simple in design and similar to those used in previous gas discharge investigations at the U.S. Naval Postgraduate School<sup>8</sup>. To facilitate pressure measurement and pumpout, the discharge tubes were connected directly to the vacuum system. A glass, three-stage, oil diffusion pump, backed by a mechanical fore pump having a capacity of 2 cu ft/min was attached to a manifold to which were connected the gas reservoir flask containing the spectroscopically pure argon gas, the discharge tube, two VG1A ionization gauges and a manometer filled with Octoil-S (conversion factor: 1 cm oil=0.672 mm Hg). Traps cooled by liquid air or liquid nitrogen were located between the discharge tube and the manifold and between the manifold and the diffusion pump. The ionization gauges were the VG1A type. A thermocouple was used to measure diffusion pump fore pressure.

The discharge tubes were purified in the standard manner of degassing the electrodes with induction heating, tube bake-out with a portable oven and finally by running a discharge and pumping down to pressures in the  $10^{-7}$  mm Hg range.

The argon was introduced into the system from the supply flask through two stopcocks with a bulb between them, thus allowing the gas to be metered into the system. The gas pressure was measured with the oil-filled manometer.



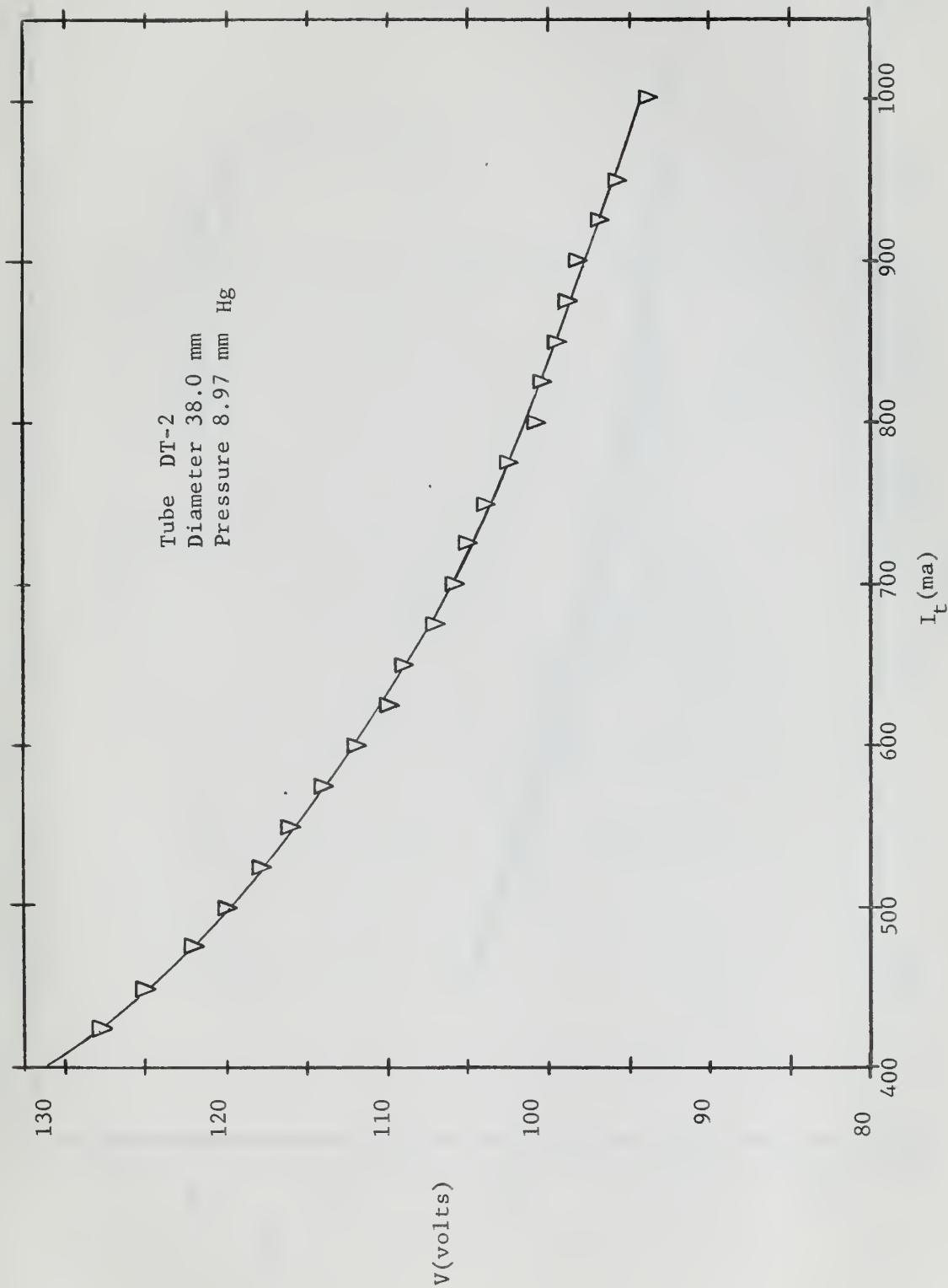


Fig. 3. Tube voltage vs tube current for DT-2.



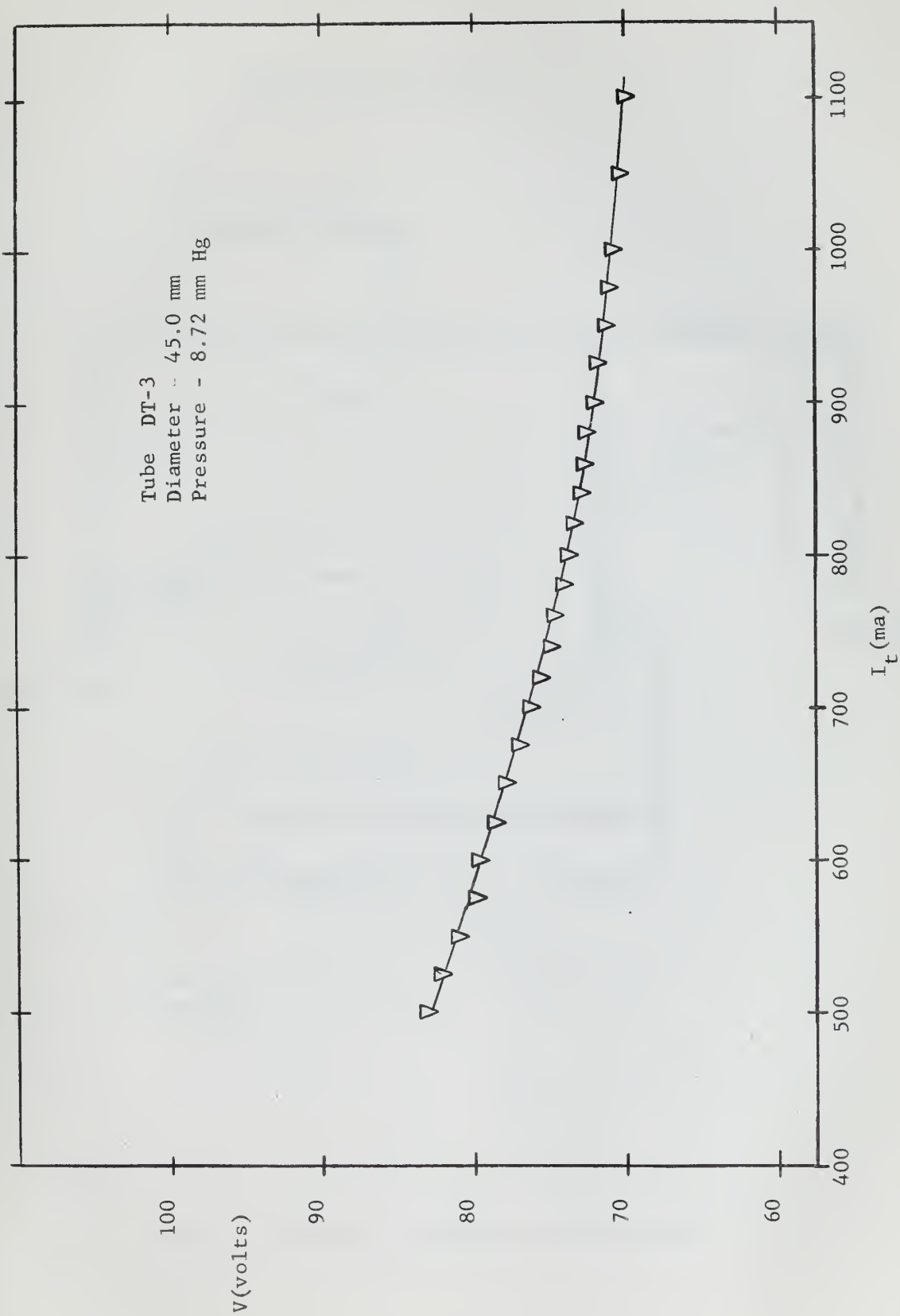


Fig. 4. Tube voltage vs tube current for DT-3





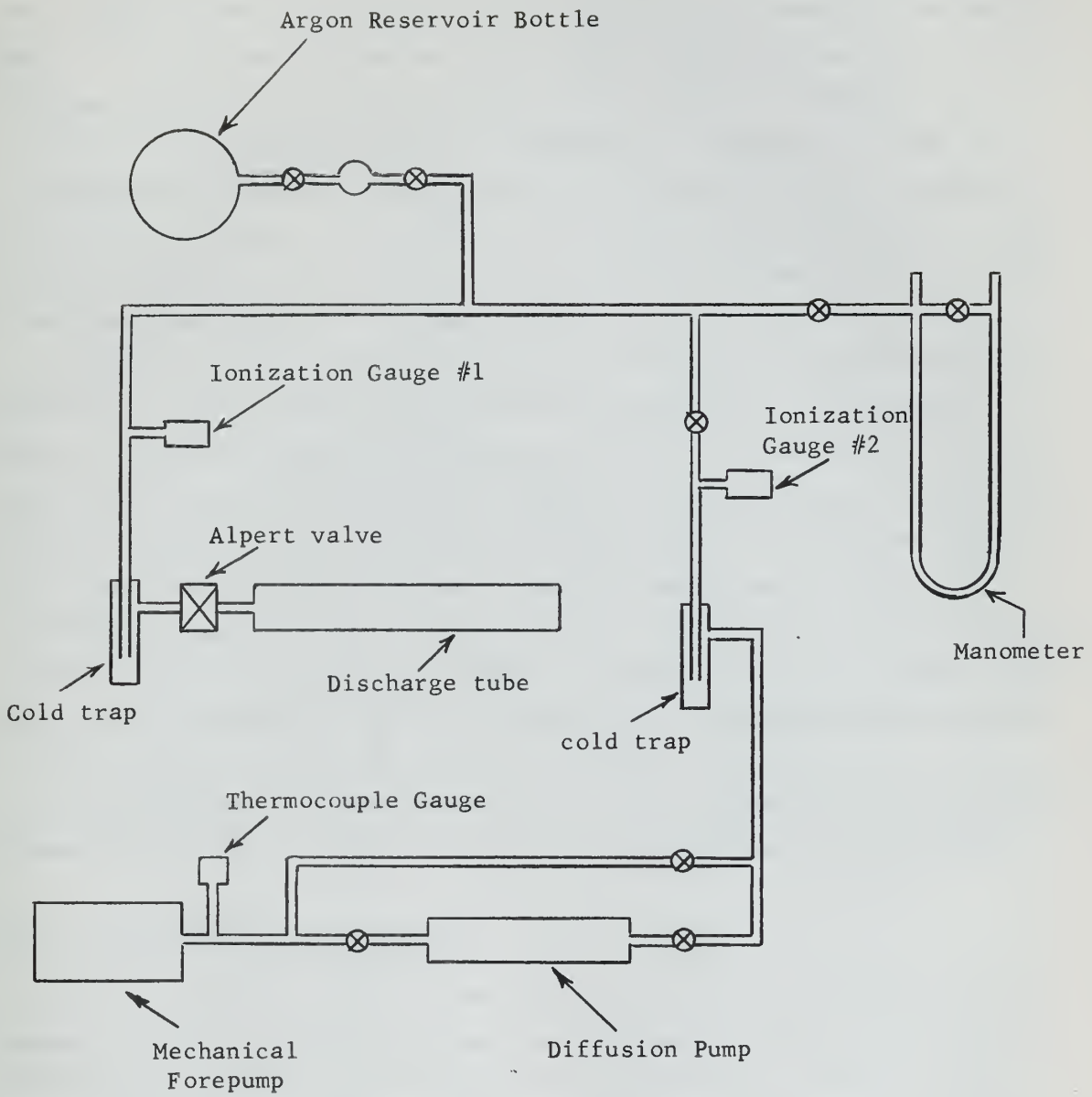


Fig. 5. Schematic diagram of vacuum system.



### 3. SPECTROGRAPHIC OBSERVATIONS

#### 3.1. SPECTROGRAPH AND ASSOCIATED OPTICAL EQUIPMENT

The spectrograph used in the spectral analysis of the gas discharge was a Baird-Atomic three meter concave grating spectrograph on an Eagle mount. The concave grating was ruled with 15,000 lines per inch. A resolving power of 50,625 in the first order, that is, a resolution of 0.1A at a wavelength of 5000A, was theoretically possible.<sup>15</sup> The spectrograph was oriented so that the discharge tube axis would be approximately perpendicular to its optical axis, the discharge tube center being aligned with the entrance slit. The physical arrangement of the spectrograph and discharge tube is shown in Fig. 6.

Two flat glass mirrors were used to reflect the beam from the end sections of the discharge tube along the optical axis of the spectrograph. Incident light was focused on a 25 micron entrance slit by a quartz lens located on the optical bench of the spectrograph and exposures could be taken in 36 different wavelength settings from 1280A to 22630A, each setting covering a range of approximately 2800A. Two of these settings were used throughout this investigation. These settings recorded wavelength ranges from 3050A to 5860A to cover the visible blue region and from 5400A to 8175A to cover the range which included several of the transitions into the metastable states of Argon I.

The detection of moving striations in the discharge was accomplished visually by means of a Central Scientific Corporation rotating mirror.

#### 3.2. PHOTOGRAPHIC PLATE ANALYSIS

Two 4 by 10 inch photographic plates were used for each set of exposures taken with the Baird-Atomic spectrograph. Kodak Spectroscopic Plates Type 1-N were used throughout the spectroscopic investigation. The type 1-N plates contained an emulsion of high sensitivity and high contrast in the visual range, being totally sensitive from approximately 2050 to 6080A and especially sensitive from 6080 to approximately 8090A. The exposed plates were developed in Kodak Developer D-19.

Analysis of the exposed plates was accomplished by using a mercury comparison spectrum and a McPherson Instrument Corporation comparator.





Fig. 6. Spectrograph/Discharge Tube Orientation





Several of the Argon I lines in each wavelength range were identified and a plate dispersion factor was calculated using the linear distance and wavelength difference between two of the identified argon lines for each exposure. By measuring the linear distance of all unknown lines from an identified argon reference line and applying the dispersion factor a computed wavelength was obtained. The dispersion factor was not quite linear but did cause an increase in the error between the computed and actual wavelength with an increase of distance from the reference line. It was possible, therefore, to take account of the increase in error when identifying the unknown spectral lines.





### 3.3. SPECTROSCOPIC PROCEDURES AND RESULTS

#### 3.3.1. Experimental Procedures

Shortly after obtaining our discharge it was evident from the appearance of the discharge that several impurities were present in the anode and cathode regions. A blue-green color was visible in the region adjacent to the cathode. This color was visible whenever the tube was in operation, the intensity of the emission depending upon the magnitude of tube current. A blue emission from the region adjacent to the anode was visible whenever the Pupp's auxiliary discharge was used regardless of whether or not the main discharge was operating. The intensity of this blue emission depended upon the voltage applied across the filament and electrode for the auxiliary discharge.

The anode and cathode regions of tube DT-1 were investigated spectroscopically. Fifteen-minute exposures were taken at approximately 3 cm from each electrode along with a five-minute exposure at the tube center with the following tube conditions: tube current 800ma, tube voltage 116v, auxiliary discharge 35ma at 170v, and tube pressure 7.8 mm Hg. Fifteen-minute exposures were also taken at approximately 5 cm and 19 cm from the cathode and at the tube center in an attempt to obtain an impurity distribution. At this time tube DT-1 failed due to melting of the filaments as mentioned in Section 2 and further exposures of this type were not taken. During all of the exposures pertaining to the impurity investigation, striations were present in the larger end sections of tube DT-1 while the smaller diameter center section was striation-free.

Tube DT-2 was a constant diameter tube, as shown in Section 2, and was the tube with which the helical instability first appeared. While taking data for the study of the helical instability, which will be described in Section 4, several sets of exposures were taken of the discharge which had the following characteristics:

1. Without helical instability
  - (a) without moving striations
  - (b) with moving striations
2. With helical instability
  - (a) without moving striations
  - (b) with moving striations



All of the exposures were taken at the tube center, between the two magnetic coils. Exposure times varied from 10 to 20 minutes for the various sets of exposures but all exposure times were the same for each set of exposures taken of the characteristics listed above. All tube parameters were approximately the same for each set of exposures with the exception of tube current. The tube current was constant for all exposures with striations but was increased to a higher constant value in order to eliminate the striations.

### 3.3.2. Analysis of the Anode Region

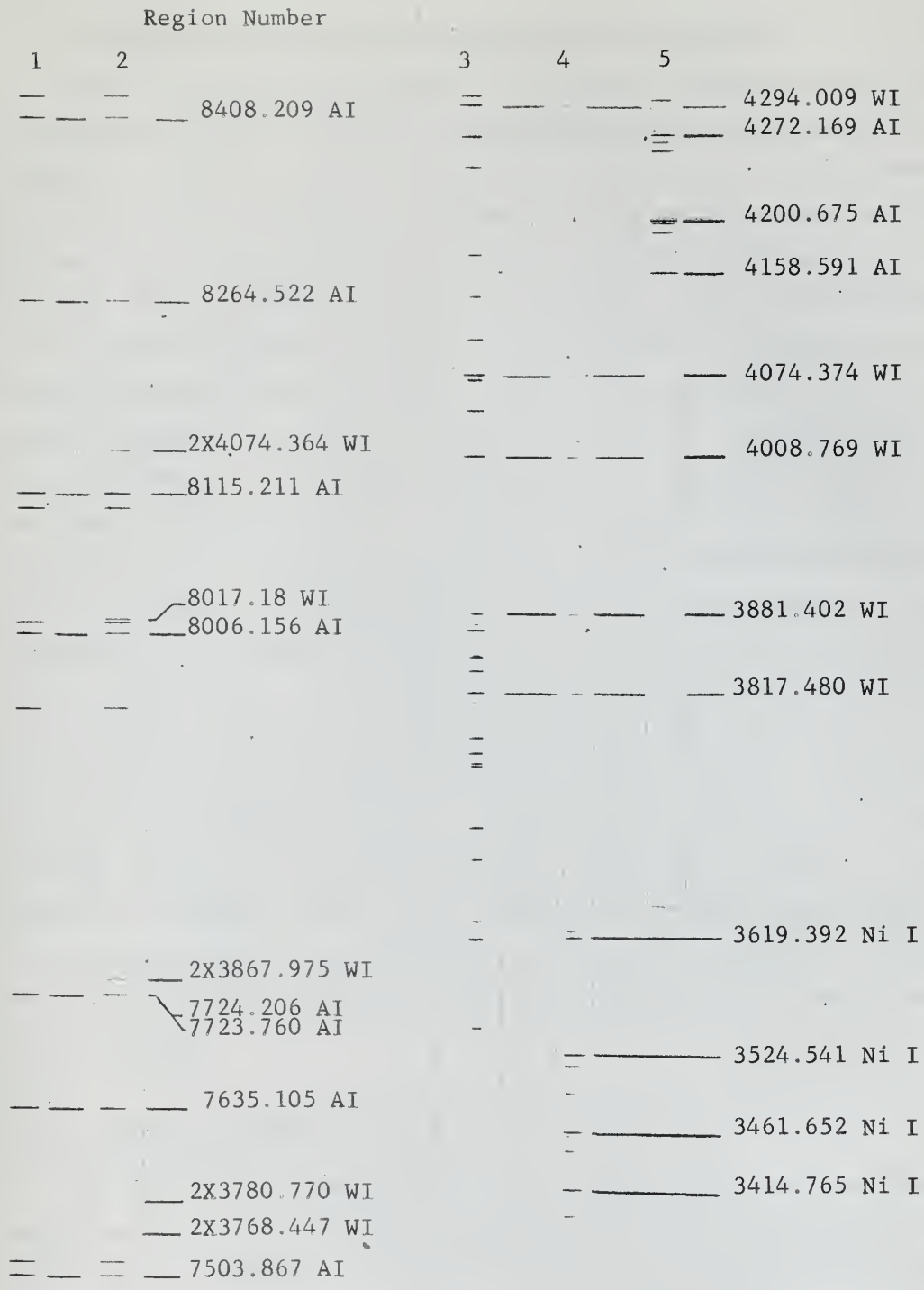
Analysis of the spectra obtained from the region approximately 3 cm from the anode-nickel electrode and tungsten filament showed a predominance of Tungsten I. Lines of Argon I were present along with the more intense lines of Nickel I. The predominance of Tungsten I was apparently due to breakdown of the argon gas between the electrode and filament and subsequent bombardment of the tungsten filament by argon ions.

### 3.3.3. Analysis of the Cathode Region

The cathode was similar to the anode in both materials and configuration but the spectra obtained were quite different. A predominance of Nickel I was seen at 3 cm and at 5 cm from the cathode with the lines of Argon I again present but only the more intense of the Tungsten I lines were seen in these two regions. The presence of Nickel I and Tungsten I was due entirely to ion bombardment of the electrode and filament by ions from the plasma beam. The predominance of Nickel I indicates that the intense sputtering, which blackened the tube walls in the cathode region<sup>2</sup>, consisted primarily of nickel atoms driven from the electrode by ion bombardment. No impurities of any kind were seen in the spectrum at 19 cm from the cathode or at the tube center.

Several examples of the spectra obtained in the investigation of the discharge are shown in Fig. 7 and all of the identified wavelengths<sup>16,17,18,19</sup> are tabulated in the Appendix.





Region Number	Region
1 & 5	Tube center
2 & 3	Anode
4	Cathode

Fig. 7. Example of discharge spectrum



### 3.3.4. Spectroscopic Notation and the Grotrian Diagrams

The transitions that produced the Argon I spectrum seen in the investigation are also included in the Appendix and are described by two different notations. The AIP (American Institute of Physics) notation consists of the following: an integer for the total quantum number  $n$ , a lower case letter denoting the orbital angular momentum of the last electron (valence electron) and two subscripts. The first subscript is the angular momentum  $K$  of the atom, exclusive of the spin of the valence electron, minus one-half. The second subscript is the total angular momentum  $J$  of the atom where  $J = K \pm 1/2$ . The levels are primed if they converge to the  ${}^2P_{1/2}$  level of the ion which lies 0.177 eV above the lowest ionization limit  ${}^2P_{3/2}$ <sup>18</sup>. The AEL (Atomic Energy Level) notation is used in both the Appendix and in the Grotrian diagrams shown in Figs. 8 and 9. In this notation the total quantum number is again indicated by an integer and is followed by the lower case designation of the optical electron. The number in brackets indicates the mean value of the  $J$  quantum numbers for a particular subgroup<sup>20</sup>. The prime used after the optical electron designation has the same meaning as that previously described for the AIP notation. An example for Argon I is the level designated  $4s' \left[ \frac{1}{2} \right]^0$  which indicates an s electron in the  $n = 4$  state where two  $J$ -values, 0 and 1, are possible—this give a mean value of  $\left[ \frac{1}{2} \right]$ —and the superscript zero indicates a term with odd parity. In the Appendix and in the Grotrian diagram of Argon I, the metastable states are indicated by an asterisk.

### 3.3.5. General Results

The lines of ionized argon did not appear in any of the exposures taken in the wavelength ranges investigated. The energy required to raise Argon I to Argon II is 15.75 electron volts. From the Grotrian diagram, it is clear that the first excited state of Argon II that would have been seen in this investigation of the visible spectrum is about 19 eV above the ground state of the ion. This is approximately 35 eV above the ground state of the neutral atom.







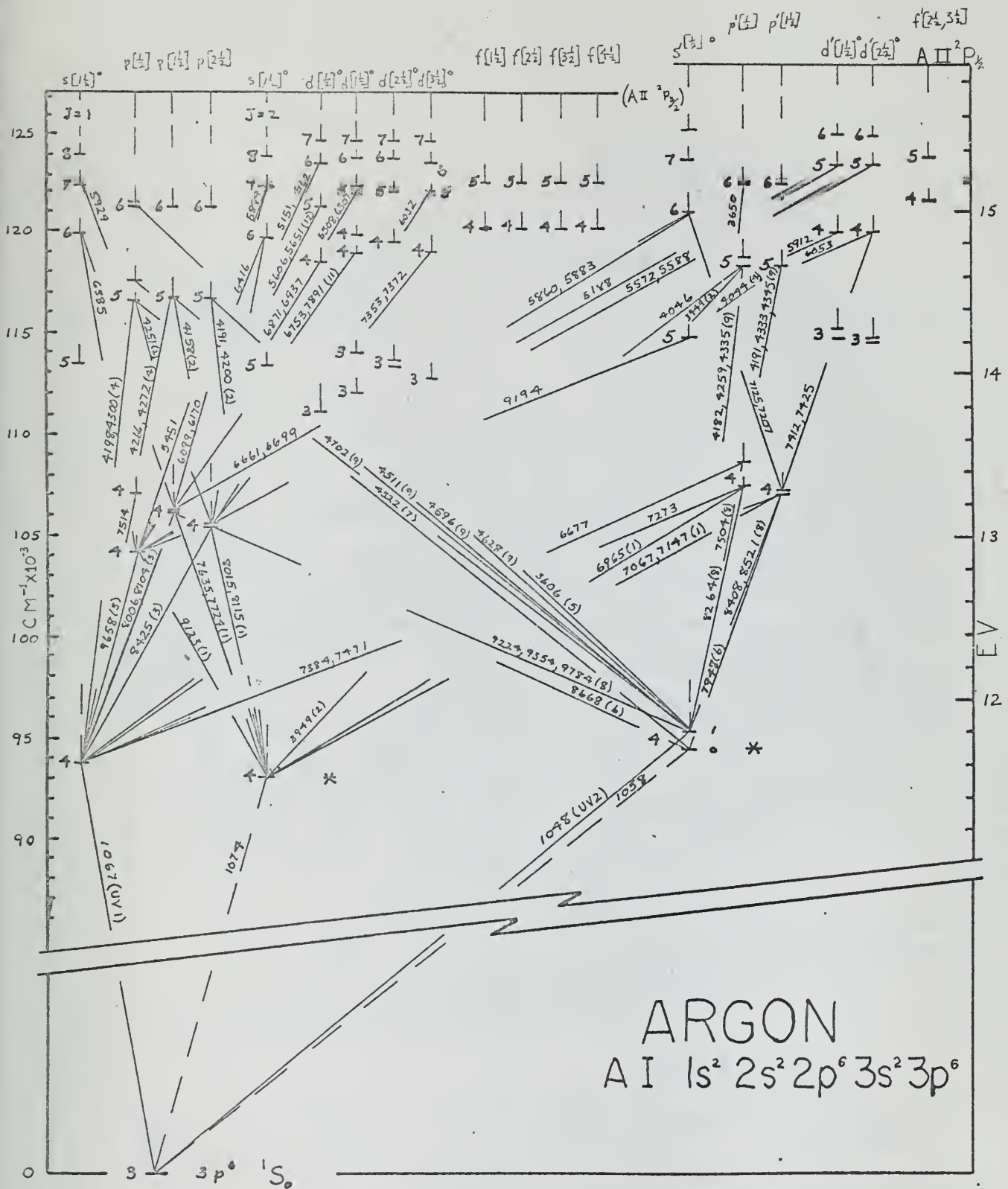


Fig. 8. Grotrian diagram of Argon I. (After R.L. Kelly, USNPS)







The highest excitation potential of Argon I observed in this research was 14.78 ev, as shown in the Appendix. From the Grotrian diagram of Argon I it can be seen that transitions from as high as 15.3 ev are possible in the 3050A-5860A range. Therefore, it seems likely that the maximum electron energy in the discharge was between 14.8 and 15.3 ev and no emission lines of ionized argon in the visible region could be expected.

No evidence of any change in the Argon I spectrum appeared in any of the exposures whether or not the positive column contained moving striations. There were no noticeable changes in relative intensity in any of the Argon I lines—in particular, those lines which are characteristic of transitions into the metastable states—and no new lines appeared in the ranges investigated. It should be mentioned, however, that at no time were exposures taken with and without striations under exactly the same conditions. Since mirrors were used to expose the end sections of the tube containing moving striations while the center section not containing striations was aligned with the spectrograph, the path lengths for the two exposures were different. The beam at the center section, which was constricted by the smaller tube cross section, was also more intense than that at the end sections. It did not seem important, therefore, to perform more conclusive tests, such as densitometer readings, in order to compare the intensities of any of the lines.

An example of the spectrum lines of the discharge under the influence of the longitudinal magnetic field are shown in Fig. 10. Again, no relative intensity changes were noticed in the wavelength ranges investigated.



Exposure Number

1            2            3            4            7383.980 AI

7503.867 AI  
7514.651 AI

7635.105 AI

7723.760 AI  
7724.206 AI

Exp. No.	Striations	Helical Instability
(1)	X	
(2)	X	X
(3)		
(4)		X

7948.175 AI

8006.156 AI  
8014.786 AI

8103.692 AI  
8115.211 AI

8264.522 AI

8408.209 AI  
8424.647 AI

8521.443 AI

Fig. 10. Argon spectrum of various discharge conditions







## 4. HELICAL INSTABILITY AND CRITICAL MAGNETIC FIELD

### 4.1. OPERATING PROCEDURES

The helical instability was investigated using tubes DT-2 and DT-3 with an externally applied magnetic field established by two helically-wound copper coils connected in series and capable of carrying currents up to 15 amperes. The coils were separated by 3 inches and were located midway between the tube ends -- Figs. 11 and 12 picture the coils and discharge tube. The power supply for the coils was a KEPCO, Model KM 236-15A; 0-15 amp, 0-50 v. A gaussmeter was used to plot a calibration curve for converting coil current to magnetic field. At the geometrical center of the arrangement the field was 225 gauss for a coil current of 15 amperes.

Prior to data-gathering runs the tube was operated until the discharge became stable. The metal Alpert valve was in the open position so that the heating effects of discharge operation would register at the manometer. The following quantities were recorded during each data-gathering run: discharge tube voltage and current,  $V_t$  and  $I_t$ , the presence and location of striations in the positive column--visually ascertained from the rotating mirror--and the critical magnetic coil current. The critical coil current was defined as that current which caused the positive column to kink and commence a sustained helical motion. Because the onset of the helical instability was determined visually, the critical coil current was subject to a slight uncertainty.

The sequence of adjustments for voltages and currents was as follows: the main power supply was set at a fixed output of 270 v, the resistor bank,  $R_1$ , was varied to give the desired tube current, then the magnetic coil current was increased until the onset of the helical instability. A range of tube currents from 400 to 1200 ma and gas pressures from 7.1 to 9.0 mm Hg was investigated.

### 4.2. RESULTS AND DISCUSSION

The plot of critical magnetic field,  $B_c$ , as a function of tube current at constant operating pressure is shown in Figs. 13 and 14. These families of curves indicate the following: the critical magnetic field increases as



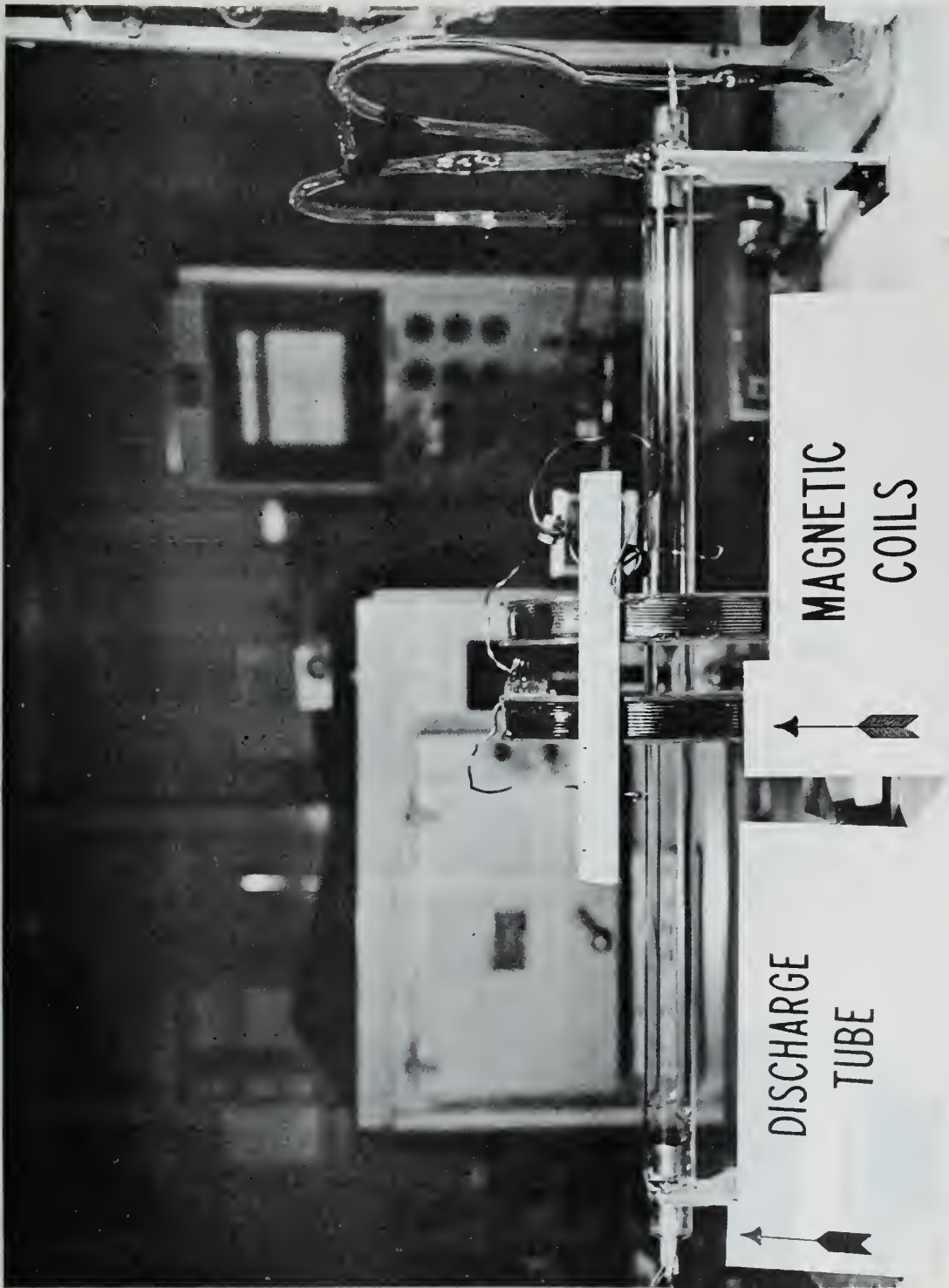


Fig. 11. Discharge tube and magnetic coil orientation (side view)



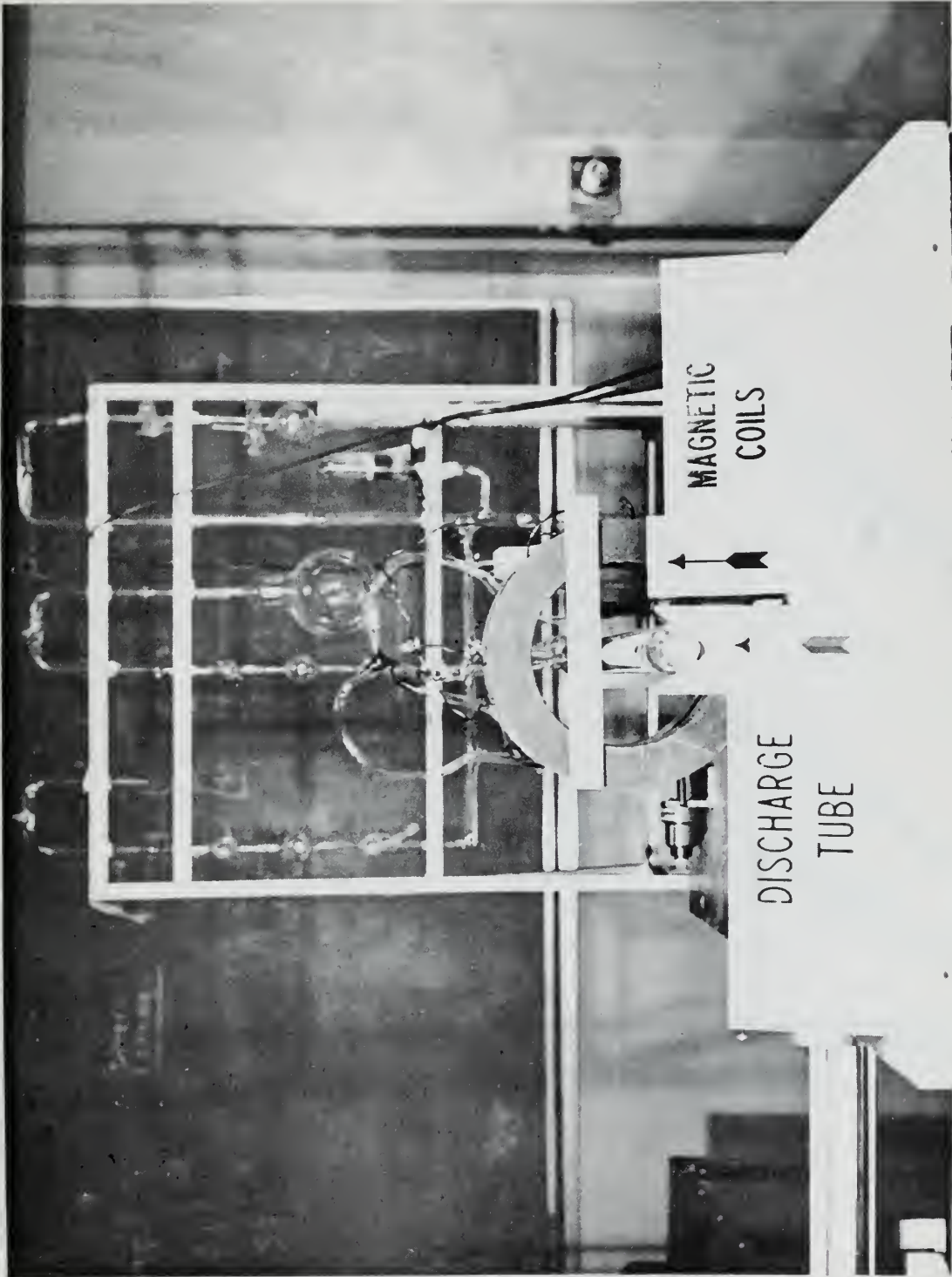
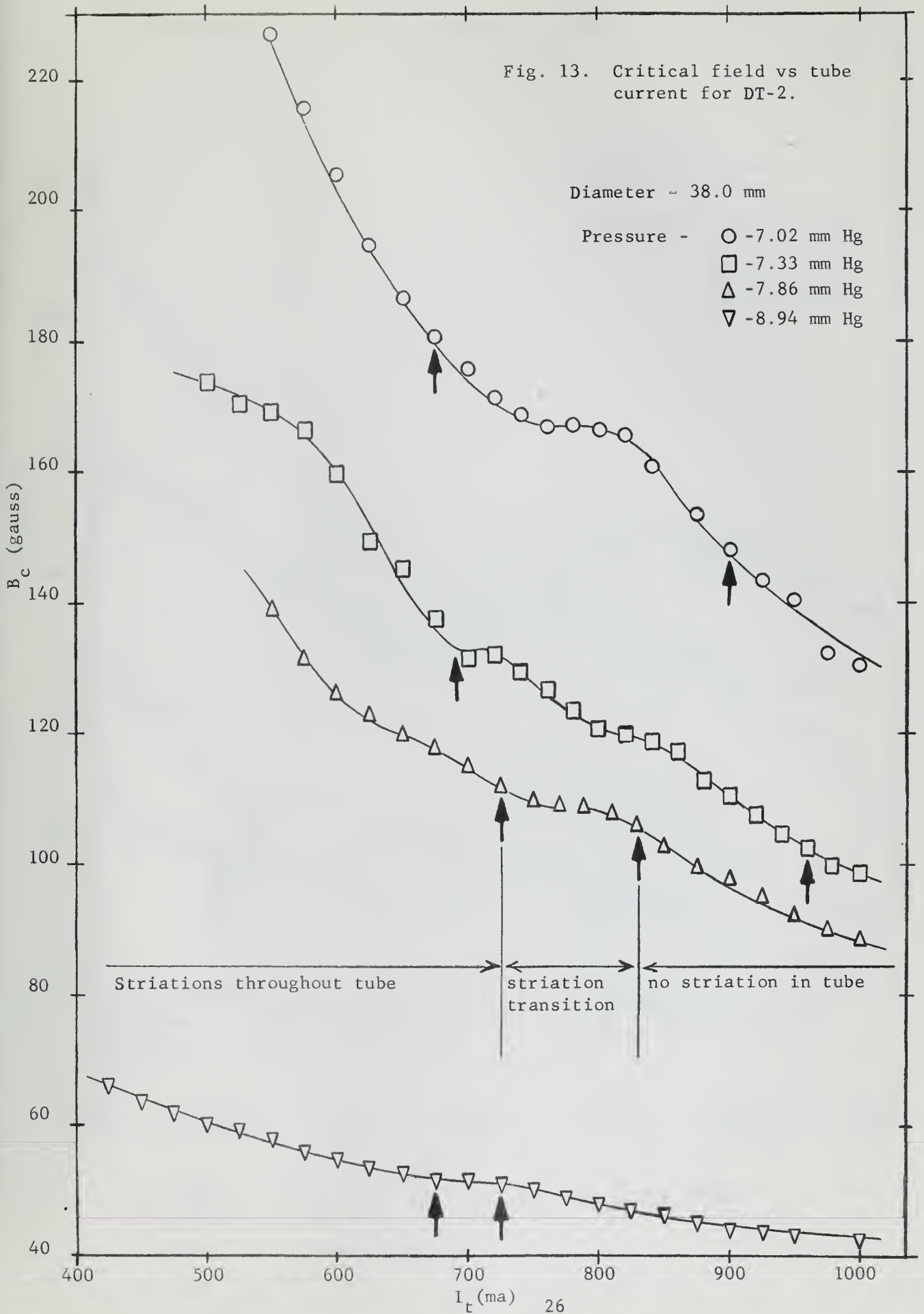


Fig. 12. Discharge tube and magnetic coil orientation (end view)





Fig. 13. Critical field vs tube current for DT-2.







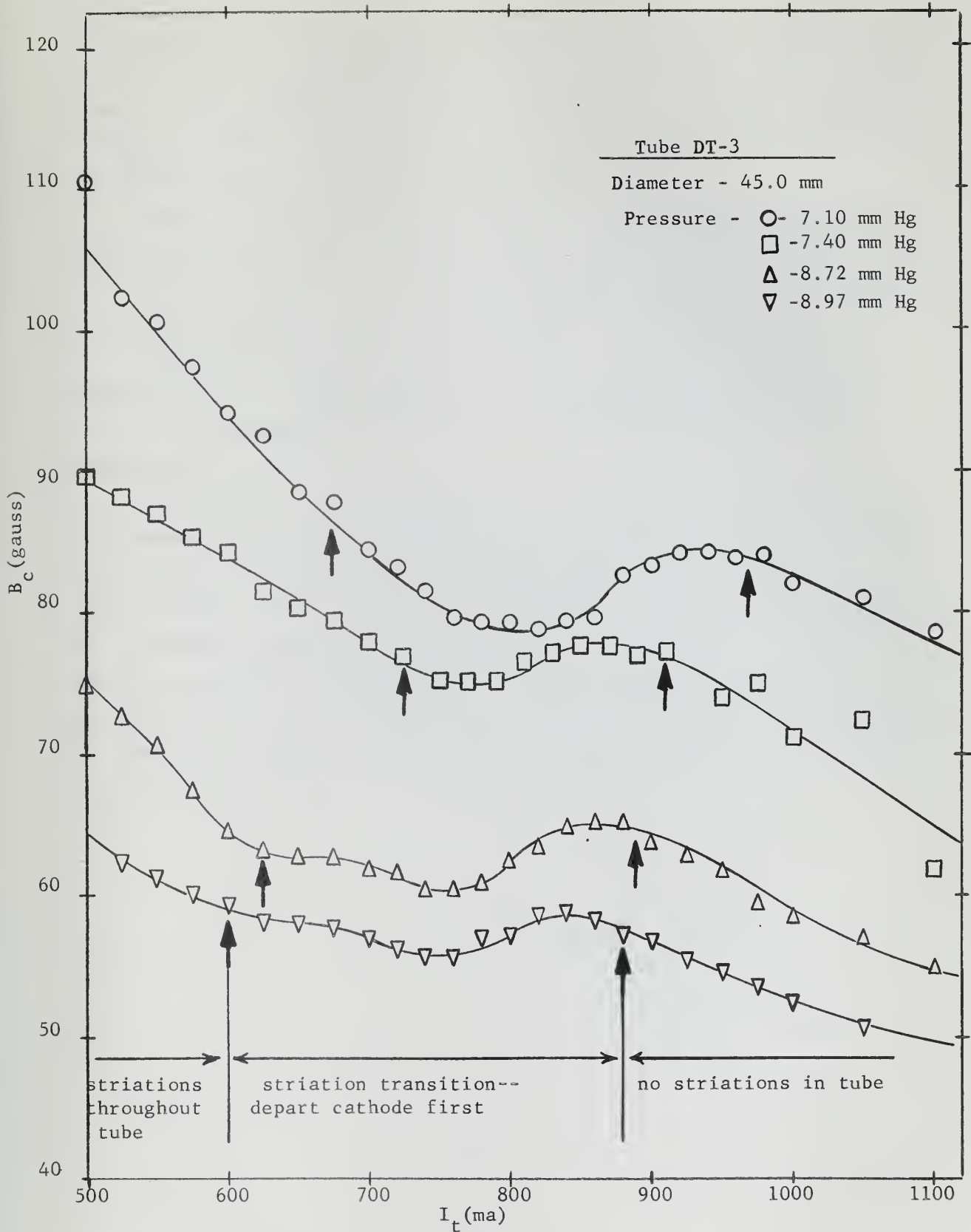


Fig. 14. Critical field vs. tube current for DT-3.



the tube radius decreases, and as the operating pressure decreases; the critical field also varies inversely as the tube current except in that range of tube currents over which the striations are disappearing from cathode to anode. There appears to exist some interaction between the striation transition and the critical field.

A plot of critical field as a function of gas pressure at constant tube current was taken from Figs. 13 and 14 and is shown in Figs. 15 and 16. The curves appear to go smoothly through transitions from unstriated to striated regimes in Fig. 15, although not so smoothly in Fig. 16.

Some of the experimental data of Figs. 15 and 16, together with calculations from the formulas of reference 10 and 11, are shown in Fig. 17. The theoretical curves were taken from the paper by Allen, Paulikas and Pyle<sup>12</sup>.

Because the inert gas and tube radii assumed in the calculation of the theoretical curves were different from those used in this experiment and because the range of pressure investigated was quite limited, it is not possible to make any definite comparisons. However, the experimental data indicate agreement more with Hoh's theory than with the theory proposed by Kadomtsev and Nadospasov. Allen, Paulikas and Pyle on the other hand obtained better agreement with the theory of Kadomtsev and Nadospasov in experiments which covered a pressure range of 0 to 8 mm Hg and a magnetic field range from 0 to 6 kilogauss.



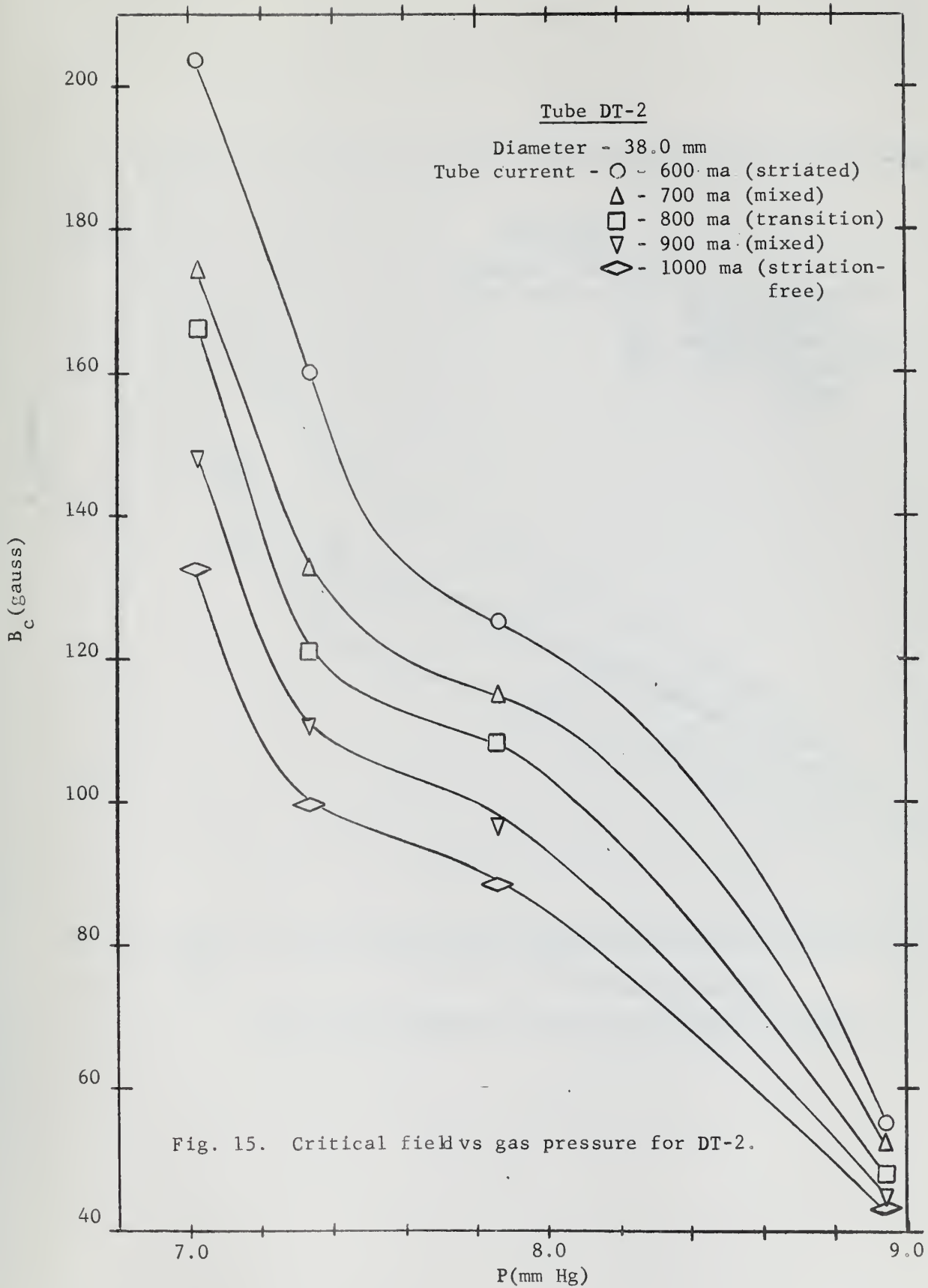


Fig. 15. Critical field vs gas pressure for DT-2.



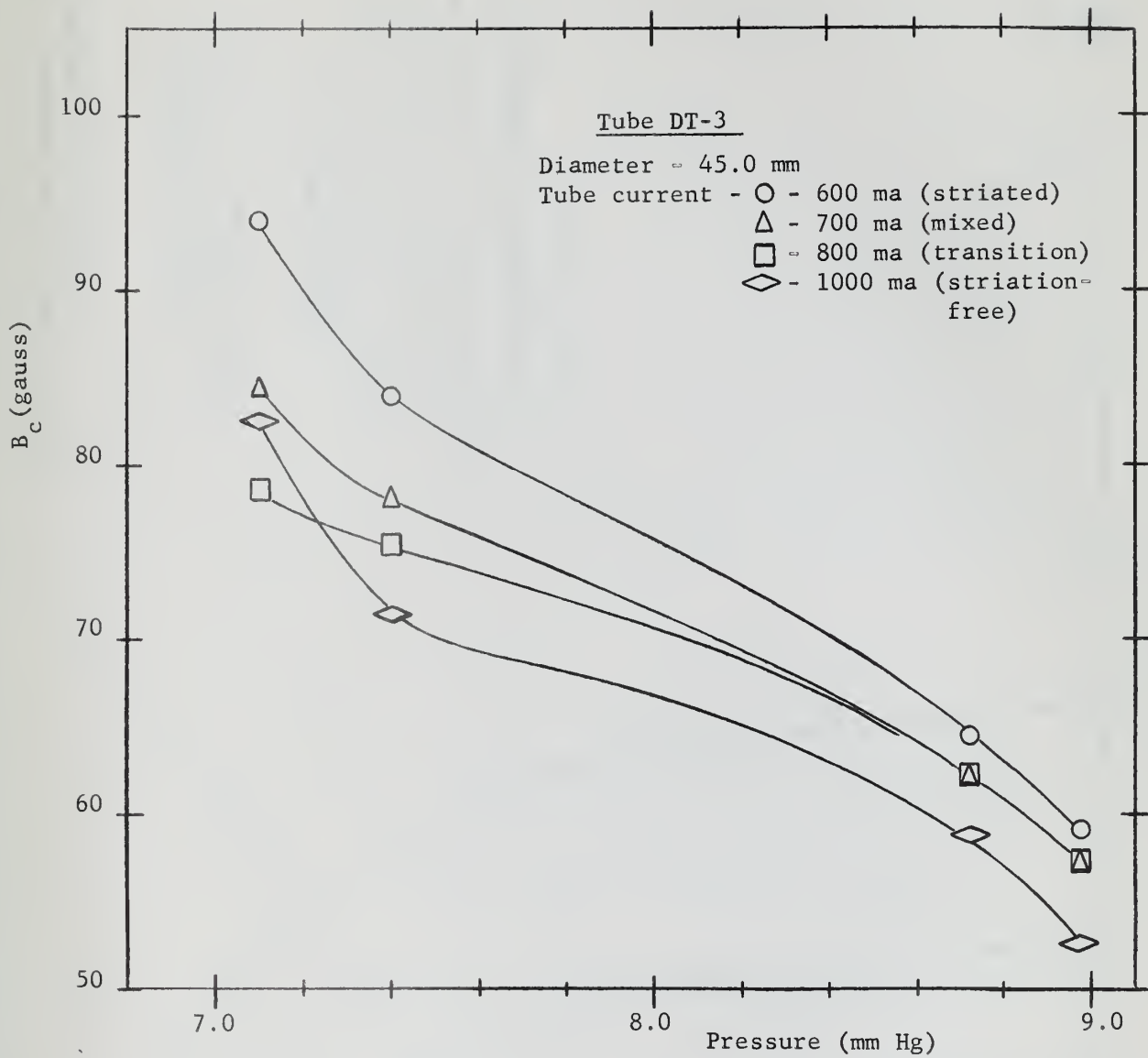


Fig. 16. Critical field vs gas pressure for DT-3.



Figure 1. Comparison of the curves for the three cases.



Fig. 17. The critical magnetic field, vs gas pressure (comparison).

Argon (experimental)

X:  $R = 2.25$  cm,  $I = 600$  ma

O:  $R = 1.90$  cm,  $I = 600$  ma

Neon (theoretical)

From Hoh's theory:

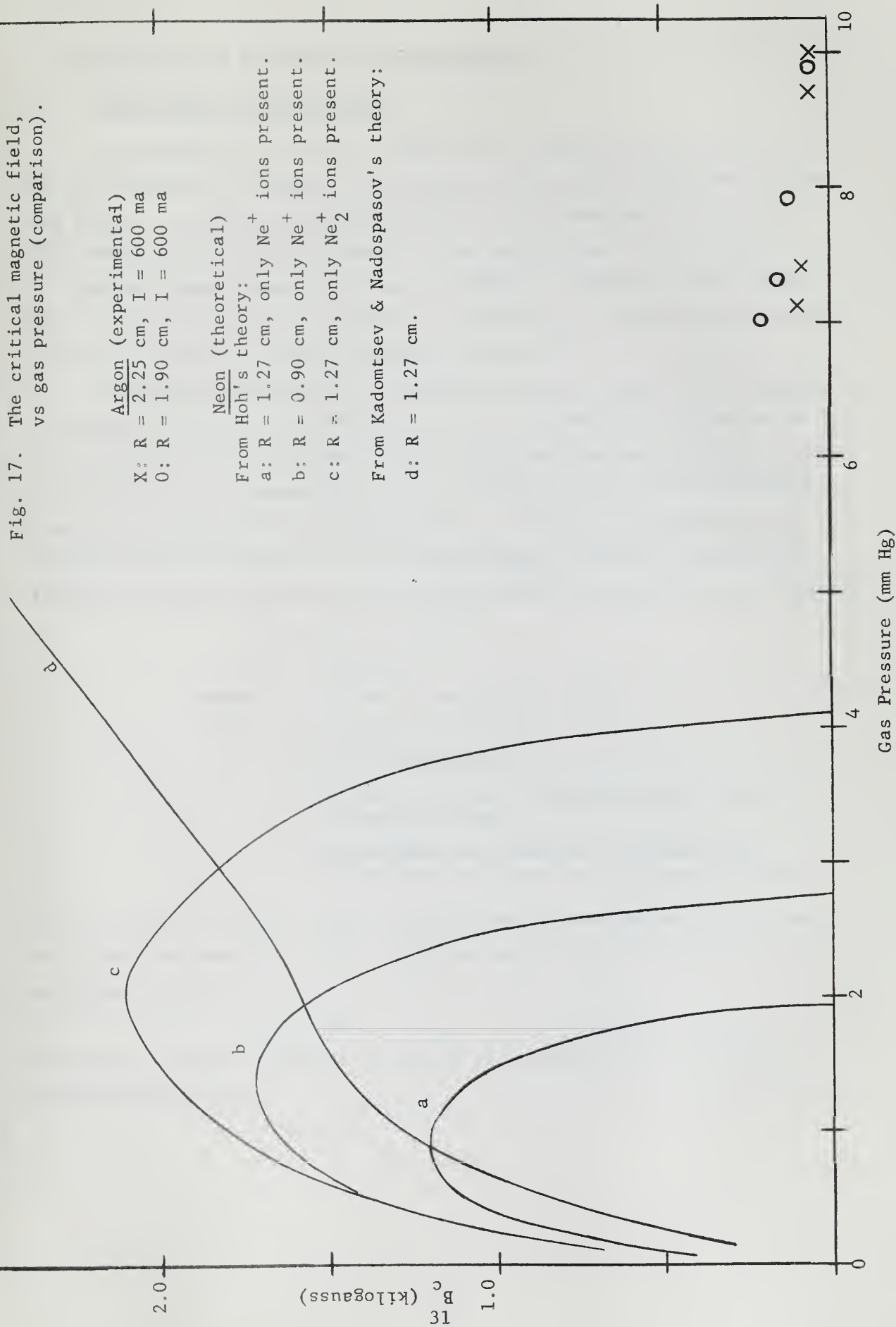
a:  $R = 1.27$  cm, only  $Ne^+$  ions present.

b:  $R = 0.90$  cm, only  $Ne^+$  ions present.

c:  $R = 1.27$  cm, only  $Ne_2^+$  ions present.

From Kadomtsev & Nadospasov's theory:

d:  $R = 1.27$  cm.





## 5. FEASIBILITY OF DOPPLER SHIFT MEASUREMENT

### 5.1. THEORETICAL CONSIDERATIONS

The technique of crossing a Fabry-Perot interferometer with an auxiliary dispersing instrument has recently been used by Zakharova, Kagan and Perel' to measure the Doppler shift of the spectrum lines, 4300A and 4044A, in an argon discharge<sup>21</sup>. The Doppler shift was observed in a rotating plasma column which had a tangential velocity of  $10^4$  cm/sec. This velocity is of the some order of magnitude as the striation velocity measured at the U.S. Naval Postgraduate School<sup>8</sup>.

By crossing a Fabry-Perot interferometer with a prism spectrograph, a Doppler shift could be detected, if one is present due to the motion of the radiating atoms which may be associated with moving striations. Consider briefly the formulation of the resolving limit and the resolving power of the Fabry-Perot interferometer. If light of wavelength  $\lambda$  is incident upon the plates of the interferometer, circular interference fringes of equal inclination are produced which are related by the equation

$$n\lambda = 2t\mu\cos\theta$$

where  $n$  = order of interference rings

$\lambda$  = incident wavelength

$t$  = plate separation

$\mu$  = refractive index of medium between interferometer plates

$\theta$  = the angular inclination of interference rings from the normal to the viewing plane

At the center of a ring system and with the interferometer plates located in air the quantity  $\mu\cos\theta$  is approximately equal to unity and the equation becomes

$$n\lambda \doteq 2t$$

Since wave number is simpler to use,  $\nu$  is introduced for  $1/\lambda$  and the equation now becomes

$$n \doteq 2t\nu$$

Faint, illegible text, possibly bleed-through from the reverse side of the page.

Second section of faint, illegible text, continuing from the top of the page.

The distance between successive fringes can be determined by differentiation and the result is

$$\Delta n = 1 \doteq 2t \Delta \nu$$

Using the Rayleigh criterion of resolution that two lines are considered resolved when their distance apart is such that the minimum intensity of the two line pattern is 0.8 of the two equal maximum intensities, Meissner<sup>22</sup> has shown that the fringe separation for two lines just resolved is

$$\Delta P \cong \frac{1}{1.49} \left( \frac{1 - R}{2\sqrt{R}} \right)$$

where  $\Delta P$  = fringe separation

R = reflection coefficient of the interferometer plates

It can be shown that this will result in a resolving limit,  $d\nu$ , of

$$d\nu \doteq \frac{1}{6t} \left( \frac{1 - R}{\sqrt{R}} \right)$$

where  $t$  = plate separation

For reflection coefficients greater than 0.90, the resolving limit  $d\nu$  becomes quite small for values of R which approach unity. For example, by using a plate separation of 1 cm and reflection coefficients of 0.90 and 0.95, the resolving limit decreases from  $0.01655 \text{ cm}^{-1}$  to  $0.0085 \text{ cm}^{-1}$ . In terms of resolving power, RP, where

$$RP = \frac{\lambda}{d\lambda} = \frac{\nu}{d\nu}$$

these reflection coefficients yield approximate values of RP of  $1.3 \times 10^6$  and  $2.4 \times 10^6$  at a wavelength of 5000A. The velocity which would be detectable using a reflection coefficient of 0.95 and a plate separation of 1 cm is approximately  $1.2 \times 10^4 \text{ cm/sec}$  from the following relationships:

$$\frac{v}{c} = \frac{d\lambda}{\lambda} = \frac{d\nu}{\nu} = \frac{1}{(RP)}$$



Present day techniques of coating Fabry-Perot interferometer plates with multiple alternating layers of dielectrics permit achievement of reflection coefficients greater than 0.99<sup>23</sup>. To take advantage of this resolving power a prism spectrograph is used to separate the wavelength incident on the interferometer.

## 5.2. INTERFEROMETER AND SPECTROGRAPH ARRANGEMENT

Much of the following material concerning the methods of crossing a Fabry-Perot interferometer with a dispersing instrument was abstracted from Chapter 9 of High Resolution Spectroscopy by S. Tolansky<sup>24</sup>.

As a dispersing instrument a prism spectrograph of either glass or quartz is preferred to a grating spectrograph because of the considerable loss of light associated with gratings. The spectrograph to be used does not have to be capable of a large dispersion since the Fabry-Perot fringes would enable the Doppler effect, if any is present, to be rapidly detected. It is common procedure to have the prism dispersion horizontal and the interferometer dispersion vertical, i.e. parallel to the spectrograph entrance slit.

Two parallel beam methods of crossing an interferometer with a spectrograph will now be examined.

### A. The external parallel beam method.

This arrangement is pictured in Fig. 18. The source S is at the focal point of an achromatic lens  $L_1$ , not necessarily of high quality. The interferometer FP is located in the parallel beam emerging from  $L_1$ . A good achromatic lens  $L_2$  projects an image of the fringes onto the slit of the spectrograph T. The fringes are dispersed by the prism P, pass through the camera lens C and onto the photographic plate.  $L_2$  needs to be an achromat only if the source consists of a number of lines of widely varying wavelength, since this lens must not produce any distortions in the fringe pattern image. The mount which holds the lenses and the interferometer must be rigid and there must be no possibility of movement with respect to the position of the slit T.



*[The text on this page is extremely faint and illegible. It appears to be a multi-column document, possibly a ledger or a list, with several columns of text and some numerical entries. The content is too blurry to transcribe accurately.]*



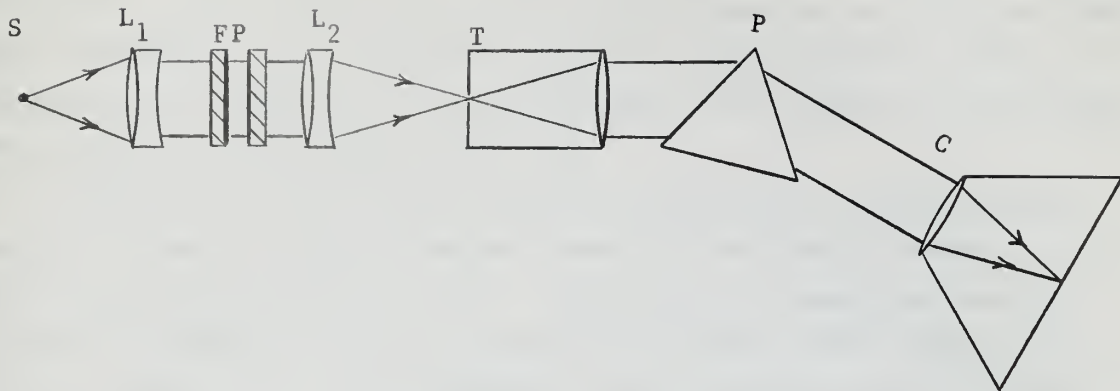
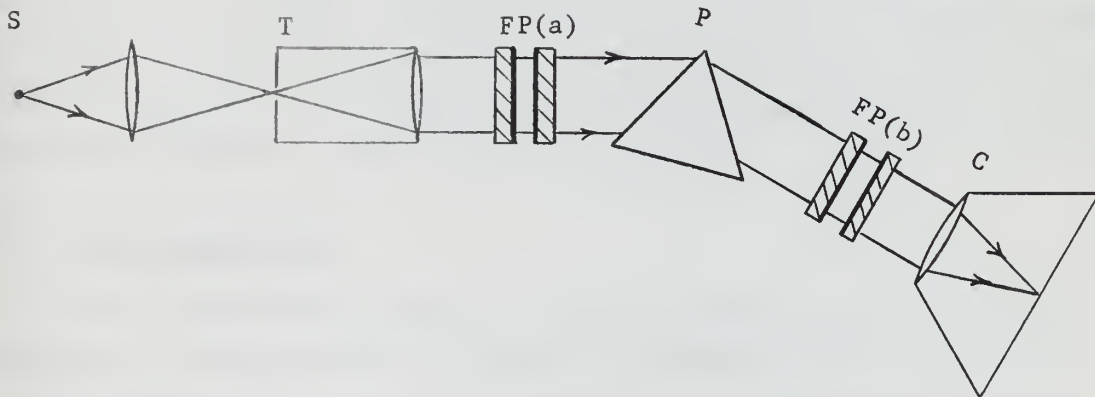


Fig. 18. Optical arrangement for interferometer - spectrograph combination - external method.



Note: The Fabry-Perot interferometer may be placed in either the (a) or (b) position.

Fig. 19. Optical arrangement for interferometer - spectrograph combination - internal method (two variations).

Handwritten text, possibly a signature or name, appearing as a series of connected loops and curves.

Handwritten text, possibly a date or a short phrase, appearing as a series of horizontal strokes.

Handwritten text, possibly a signature or name, appearing as a series of connected loops and curves.

Handwritten text, possibly a date or a short phrase, appearing as a series of horizontal strokes.

Handwritten text, possibly a date or a short phrase, appearing as a series of horizontal strokes.

## B The internal parallel beam method.

A quite simple method of crossing an interferometer with a prism spectrograph is the internal parallel beam method of which there are two variations. These variations of the internal mounting in which the Fabry-Perot interferometer is introduced inside the spectrograph, either: (a) between the collimating lens and the prism, or (b) between the prism and the camera lens, are shown in Fig. 19.

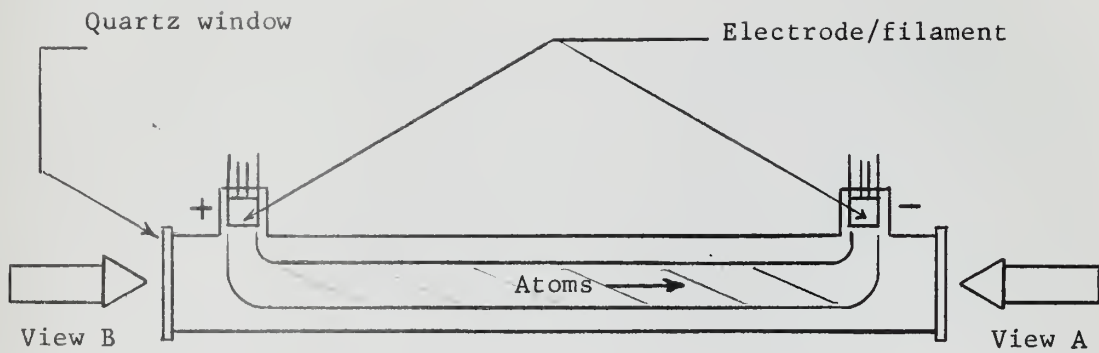
Compared with the external parallel beam method, there are advantages to using the internal method; these are: achromatic lenses  $L_1$  and  $L_2$  in Fig. 18 are dispensed with — especially the expensive lens  $L_2$ , because the fringes are now projected by the high quality camera lens — light is conserved by the elimination of the two lenses and the labor of determining accurate focal positions for lens  $L_2$  is avoided. However, there is one distinct disadvantage of internal method (b); this is, the range of measurable wavelengths is considerably restricted. Although the light beams entering the prism are parallel, the emerging beams belonging to different wavelengths strike the interferometer at different angles of incidence. For example, if the light of the wavelength which suffers minimum deviation falls normally upon the interferometer plates, the light from any other wavelength will have an angle of incidence other than normal. Position (b) is less favorable than position (a) but for a complete treatment of the advantages and disadvantages of various crossing methods Tolansky's book should be consulted.

### 5.3. TUBE CONSTRUCTION

A tube construction similar to that pictured in Fig. 20 might be employed in conjunction with the optical equipment of sub-section 5.2. Moving striations have been observed with a tube configuration similar to this one, and the advantage of the off-axis electrode/filament lies in the ability to view the discharge column axially without the obstructions presented by the more conventional electrode/filament arrangements shown in sub-section 2.1.

Because of the small axial velocity components anticipated, the tube should be viewed from each end. The delicate adjustments required for





View A - Doppler shift of  $\lambda - d\lambda$   
 View B - Doppler shift of  $\lambda + d\lambda$

Fig. 20. Tube construction.



Faint, illegible text or a title centered below the illustration.

the Fabry-Perot interferometer dictate the use of mirrors rather than a movement of the optical equipment when viewing each end of the tube.





## 6. CONCLUSIONS

### 6.1. CONCLUSIONS

#### A. Spectroscopic

The spectroscopic investigation of the positive column indicated that there were no noticeable intensity changes of any of the Argon I lines and that no new lines appeared in the wavelength ranges investigated when comparing (a) the striated and striation-free column, or (b) the stable column and the column with the helical instability both with and without striations.

No argon ion spectrum in the visible region was observed at any time, indicating that the maximum electron energy was not high enough to ionize and excite the argon atoms in order to obtain a visible spectrum; that is, the maximum electron energy was less than about 19 ev.

Impurities were cast into the system by ion bombardment of the electrodes and filaments. The impurities did not, however, penetrate into the positive column to any great extent, at least not as far as 19 cm from the cathode. The effect of the impurities on the stability of the system is unknown but no apparent effect was noticed.

#### B. Helical instability

The critical magnetic field for the onset of the helical instability is sensitive to changes in the system parameters of discharge tube radius and current and changes in gas pressure. There is an apparent interaction between the critical field and the transition of the discharge from the striated to striation-free regime.

The experimental results showed some agreement with one theory concerning the helical instability.

#### C. Doppler shift measurement

Using a Fabry-Perot interferometer and prism spectrograph, it should be possible to measure atom velocities in a discharge tube if these velocities were equal to or greater than previously measured striation velocities.

Section 1

Section 2

The first section of the report discusses the background and objectives of the study. It highlights the importance of understanding the current state of the industry and the challenges it faces. The second section provides a detailed overview of the methodology used in the research, including the data sources and the analytical tools employed.

The third section presents the findings of the study, which show a significant trend towards digitalization and automation in the sector. This is driven by the need for efficiency and cost reduction. The fourth section discusses the implications of these findings for stakeholders, including policymakers and industry leaders.

The fifth section offers recommendations for addressing the challenges identified in the study. It suggests that a combination of government support and industry innovation is necessary to foster a more resilient and competitive environment. The final section concludes the report by summarizing the key points and reiterating the need for continued research and collaboration.

Section 3

This section delves into the specific challenges faced by small and medium-sized enterprises (SMEs) in the industry. It identifies the lack of access to capital and talent as major barriers to growth. The text also discusses the impact of global economic fluctuations and trade tensions on the sector's performance.

The following section explores the role of government in supporting the industry's development. It examines various policy options, such as tax incentives and grants, and evaluates their effectiveness. The text also discusses the importance of regulatory reform in creating a more favorable business environment.

Section 4

The final section of the report provides a comprehensive overview of the industry's future prospects. It highlights the potential for growth and innovation, particularly in the areas of artificial intelligence and data analytics. The text also discusses the need for a strong and skilled workforce to support this growth.

## 6.2. RECOMMENDATIONS

In order to further the research in the field of gas discharge presently being conducted at USNPS the following recommendations for future work are offered.

A time-resolved spectroscopic investigation of the visible radiation emitted from a striated discharge should be made using a shuttering technique. This would eliminate the integrated effects of continuous viewing that were encountered in these experiments.

The investigation of the helical instability should be continued using variations in tube diameter, higher magnetic field and lower tube current in order to provide more complete data for comparison with present theories.

An attempt should be made to measure the Doppler effect of moving atoms in a discharge, if any motion is present, to establish an inter-relationship of atom motion and the phenomenon of moving striations.



## REFERENCES

1. Sanborn C. Brown, Basic Data of Plasma Physics, (The Technology Press and Wiley and Sons, Inc., New York, 1959), Chap. 14.
2. Gordon Francis, The Glow Discharge at Low Pressure, (Handbuch der Physik, Springer-Verlag, 1956), Vol. XXII, p.53.
3. K.B. Emeleus, The Conduction of Electricity Through Gases, (John Wiley and Sons, Inc., New York, 1951).
4. W. Pupp, Physik.Z.33,844(1932);34,756(1933);35,705(1934);36,61(1935)  
Z. Tech. Phys. 7,257(1934).
5. T. Donahue and G.H. Dieke, Phys. Rev. 81, 248 (1951).
6. H.S. Robertson, Phys. Rev. 105, 368 (1957).
7. L. Pekarek, Phys. Rev. 1371 (1957). Czech. J. Phys. 4,221(1954);  
7,533(1957); 8,32(1958).
8. A.W. Cooper, Moving Striations in the Inert Gases, (Ph.D. Thesis, Queens University of Belfast, 1961).
9. F.C. Hoh and B. Lehnert, Phys. Fluids 3, 600 (1960).
10. F.C. Hoh, Phys. Rev. Letters 4,559 (1960).
11. B.B. Kadomtsev and A.V. Nedospasov, J. Nuclear Energy, Part C1,230 (1960).
12. T.K. Allen, G.A. Paulikas and R.V. Pyle, Phys. Rev. Letters 5,409(1960).
13. R.N. Habermehl and D.A. Hughes, Moving Striations and Anode Effects in an Argon Glow Discharge, (M.S. Thesis, U.S. Naval Postgraduate School, 1961).
14. W. Pupp, Physik. Z. 34, 756 (1933).
15. Instruction Manual for Baird-Atomic Three Meter Grating Spectrograph-- Model GX-1.
16. Charlotte E. Moore, A Multiplet Table of Astrophysical Interest, National Bureau of Standards, Technical Note 36, Nov 1959, distributed by U.S. Department of Commerce.
17. Massachusetts Institute of Technology Wavelength Tables, (The Technology Press, John Wiley & Sons, Inc., New York).
18. American Institute of Physics Handbook, (McGraw-Hill Book Company, Inc., New York, 1957).



19. A.N. Zaidel', V.K. Prokof'ev and S.M. Raiskii, Tables of Spectrum Lines, (Pergamon Press, New York, 1961).
20. Charlotte E. Moore, Atomic Energy Levels, Vol. I, National Bureau of Standards Circular 467, June 15, 1949, U.S. Department of Commerce.
21. V.M. Zakharova, Y.M. Kagan and V.I. Perel', Optics and Spectroscopy, 11, 421 (1961).
22. K.W. Meissner, J. Opt. Soc. Am. 31, 405 (1941).
23. P. Baumeister, J. Opt. Soc. Am. 48, 955 (1958).
24. S. Tolansky, High Resolution Spectroscopy, (Pitman Publishing Corp., New York, 1945), Chap. 9.





APPENDIX

Identified Wavelengths

ARGON I									
Wavelength (Angstroms)	Intensity (log I) &	Region Seen $\zeta$	Transition						Excitation Energy Above Ground State (ev)
			AIP		AEL				
			Upper State	Lower State	Upper State	J	Lower State	J	
3947.505	1.54	2,3	5p <sub>12</sub> '	4s <sub>12</sub>	5p' [1 1/2]	2	4s [1 1/2] <sup>o</sup>	2	14.62
3948.979	3.09	2,3,4,5	5p <sub>01</sub> '	4s <sub>12</sub>	5p' [1/2]	1	4s [1 1/2] <sup>o</sup>	2	14.62
4044.418	3.16	2,3,4,5	5p <sub>12</sub> '	4s <sub>11</sub>	5p' [1 1/2]	2	4s [1 1/2] <sup>o</sup>	1	14.62
4158.591	3.80	1,2,3,4,5	5p <sub>12</sub>	4s <sub>12</sub>	5p [1 1/2]	2	4s [1 1/2] <sup>o</sup>	2	14.47
4164.179	3.03	2,3,4,5	5p <sub>11</sub>	4s <sub>12</sub>	5p [1 1/2]	1	4s [1 1/2]	2	14.46
4181.883	3.13	2,3	5p <sub>01</sub> '	4s <sub>00</sub> '	5p' [1/2]	1	4s' [1/2] <sup>o</sup>	0	14.62
4190.713		2,3	5p <sub>22</sub>	4s <sub>12</sub>	5p [2 1/2]	2	4s [1 1/2] <sup>o</sup>	2	14.44
4191.029		1,2,3	5p <sub>11</sub> '	4s <sub>00</sub> '	5p' [1 1/2]	1	4s' [1/2] <sup>o</sup>	0	14.62
4198.317	3.53	1,2,3,4,5	5p <sub>00</sub>	4s <sub>11</sub>	5p [1/2]	0	4s [1 1/2] <sup>o</sup>	1	14.51
4200.675	3.83	1,2,3,4,5	5p <sub>23</sub>	4s <sub>12</sub>	5p [2 1/2]	3	4s [1 1/2] <sup>o</sup>	2	14.44
4259.362	3.40	1,2,3,4,5	5p <sub>00</sub> '	4s <sub>01</sub> '	5p' [1/2]	0	4s' [1/2] <sup>o</sup>	1	14.67
4266.286	3.29	1,2,3,4,5	5p <sub>12</sub>	4s <sub>11</sub>	5p [1 1/2]	2	4s [1 1/2] <sup>o</sup>	1	14.47
4272.169	3.54	1,2,3,4,5	5p <sub>11</sub>	4s <sub>11</sub>	5p [1 1/2]	1	4s [1 1/2] <sup>o</sup>	1	14.46
4300.101	3.40	1,2,3,4,5	5p <sub>00</sub>	4s <sub>11</sub>	5p [1/2]	0	4s [1 1/2] <sup>o</sup>	1	14.44
4333.561	3.32	1,2,3,4,5	5p <sub>12</sub> '	4s <sub>01</sub> '	5p' [1 1/2]	2	4s' [1/2] <sup>o</sup>	1	14.62
4335.337	2.95	1,2,3,4,5	5p <sub>01</sub> '	4s <sub>01</sub> '	5p' [1/2]	1	4s' [1/2] <sup>o</sup>	1	14.62
4345.168	2.91	2,3,4,5	5p <sub>11</sub> '	4s <sub>01</sub> '	5p' [1 1/2]	1	4s' [1/2] <sup>o</sup>	1	14.62
4510.733	3.13	2,3,4,5	5p <sub>00</sub>	4s <sub>01</sub> '	5p [1/2]	0	4s' [1/2] <sup>o</sup>	1	14.51
4522.323	2.62	2,3	5p <sub>01</sub>	4s <sub>00</sub> '	5p [1/2]	1	4s' [1/2] <sup>o</sup>	0	14.40
4596.046	2.65	2,3	5p <sub>11</sub>	4s <sub>01</sub> '	5p [1 1/2]	1	4s' [1/2] <sup>o</sup>	1	14.46
6965.430	5.06	1,2,3,4,5	4p <sub>01</sub> '	4s <sub>12</sub>	4p' [1/2]	1	4s [1 1/2] <sup>o</sup>	2	13.27
7067.217	5.01	1,2,3,4,5	4p <sub>12</sub> '	4s <sub>12</sub>	4p' [1 1/2]	2	4s [1 1/2] <sup>o</sup>	2	13.24
7147.041	4.42	1,2,3	4p <sub>11</sub> '	4s <sub>12</sub>	4p' [1 1/2]	1	4s [1 1/2] <sup>o</sup>	2	13.23
7272.935	4.71	1,2,3	4p <sub>01</sub> '	4s <sub>11</sub>	4p' [1/2]	1	4s [1 1/2] <sup>o</sup>	1	13.27
7372.119	3.76	2,3,4,5	4d <sub>34</sub>	4p <sub>23</sub>	4d [3 1/2] <sup>o</sup>	4	4p [2 1/2]	3	14.78



ARGON I

Wave length (Angstroms)	Intensity (log I) &	Region Seen $\zeta$	Transition						Excitation Energy Above Ground State (ev)
			AIP		AEL				
			Upper State	Lower State	Upper State	J	Lower State	J	
7383.980	5.02	1,2,3,4,5	5p' <sub>12</sub>	4s <sub>11</sub>	4p' $\overline{1\ 1/2}$	2	4s $\overline{1\ 1/2}$ °	1	13.23
7503.867	5.35	1,2,3,4,5	4p' <sub>00</sub>	4s' <sub>01</sub>	4p' $\overline{1/2}$	0	4s' $\overline{1/2}$ °	1	13.42
7514.651	5.22	1,2,3,4,5	4p <sub>00</sub>	4s <sub>11</sub>	4p $\overline{1/2}$	0	4s $\overline{1\ 1/2}$ °	1	13.23
* 7635.105	5.53	1,2,3,4,5	4p <sub>12</sub>	4s <sub>12</sub>	4p $\overline{1\ 1/2}$	2	4s $\overline{1\ 1/2}$ °	2	13.11
7723.760	5.44	1,2,3,4,5	4p <sub>11</sub>	4s <sub>12</sub>	4p' $\overline{1/2}$	1	4s $\overline{1\ 1/2}$ °	2	13.10
* 7724.206		1,2,3,4,5	4p <sub>11</sub>	4s <sub>12</sub>	4p $\overline{1\ 1/2}$	1	4s $\overline{1\ 1/2}$ °	2	13.27
* 7948.175	5.13	1,2,3,4,5	4p' <sub>11</sub>	4s' <sub>00</sub>	4p' $\overline{1\ 1/2}$	1	4s' $\overline{1/2}$ °	0	13.23
8006.156	5.23	1,2,3,4,5	4p <sub>12</sub>	4s <sub>11</sub>	4p $\overline{1\ 1/2}$	2	4s $\overline{1\ 1/2}$ °	1	13.11
* 8014.786	5.30	1,2,3,4,5	4p <sub>22</sub>	4s <sub>12</sub>	4p $\overline{2\ 1/2}$	2	4s $\overline{1\ 1/2}$ °	2	13.04
8103.692	5.31	1,2,3,4,5	4p <sub>11</sub>	4s <sub>11</sub>	4p $\overline{1\ 1/2}$	1	4s $\overline{1\ 1/2}$ °	1	13.10
* 8115.311	5.58	1,2,3,4,5	4p <sub>23</sub>	4s <sub>12</sub>	4p $\overline{2\ 1/2}$	3	4s $\overline{1\ 1/2}$ °	2	13.02
8127.30		2,3,4,5							
8264.522	5.28	1,2,3,4,5	4p' <sub>01</sub>	4s' <sub>01</sub>	4p' $\overline{1/2}$	1	4s' $\overline{1/2}$ °	1	13.27
# 2X4158591		2,3,4,5	5p <sub>12</sub>	4s <sub>12</sub>	5p $\overline{1\ 1/2}$	2	4s $\overline{1\ 1/2}$ °	2	14.47
# 2X4198.37		4,5	5p <sub>00</sub>	4s <sub>11</sub>	5p $\overline{1/2}$	0	4s $\overline{1\ 1/2}$ °	1	14.51
# 2X4200675		2,3	5p <sub>23</sub>	4s <sub>12</sub>	5p $\overline{2\ 1/2}$	3	4s $\overline{1\ 1/2}$ °	2	14.44
8408.209	5.36	1,2,3,4,5	4p' <sub>12</sub>	4s' <sub>01</sub>	4p' $\overline{1\ 1/2}$	2	4s $\overline{1/2}$ °	1	13.24
8424.647	5.35	1,2,3,4,5	4p <sub>22</sub>	4s <sub>11</sub>	4p $\overline{2\ 1/2}$	2	4s $\overline{1\ 1/2}$ °	1	13.04
8521.443	5.18	1,2,3,4,5	4p' <sub>11</sub>	4s' <sub>01</sub>	4p' $\overline{1\ 1/2}$	1	4s' $\overline{1/2}$ °	1	13.23



NICKEL I

Wavelength (angstroms)	Intensity <sup>&amp;</sup>	Region Seen <sup>ç</sup>
3050.819	1000	4
3101.554	1000	4
3134.108	1000	4
3232.963	300	4
3369.573	500	4
3371.993	400	4
3380.574	600	4
3391.050	400	4
3392.992	600	4
3414.765	1000	4
3423.711	600	4
3433.558	800	4
3437.280	600	4
3446.263	1000	4
3452.890	600	4
3458.474	800	4
3461.652	800	1,4
3467.502	300	4
3483.774	500	4
3492.956	1000	1,4
3510.338	900	1,4
3515.054	1000	1,4
3524.541	1000	1,4
3561.751		4
3566.372	2000	1,4
3571.869	1000	4
3587.931	200	4
3609.314	200	4
3612.741	400	4
3619.392	2000	1,4
3624.733	150	4
3674.15	200	4



Wavelength (angstroms)	Intensity <sup>&amp;</sup>	Region Seen <sup>ç</sup>
3749.045		4
3783.530	500	4
3807.144	800	4
3858.301	800	4
3912.979		4
# 2X2994.460	125	4
# 2X3002.491	1000	4
# 2X3003.629	500	4
# 2X3012.004	800	4
# 2X3037.935	800	4
# 2X3050.819	1000	4
# 2X3054.316	400	4
# 2X3101.554	1000	4
# 2X3101.879	400	4
# 2X3107.714		4
# 2X3232.963	300	4
# 2X3369.573	500	4
# 2X3371.993	400	4
# 2X3380.574	600	4
# 2X3391.050	400	4
# 2X3392.992	600	4
# 2X3414.765	1000	1,4
# 2X3423.711	600	4
# 2X3433.558	800	4
# 2X3437.280	600	4
# 2X3446.263	1000	4
# 2X3452.890	600	4
# 2X3458.474	800	4
# 2X3461.652	800	1,4
# 2X3472.545	800	4
# 2X3492.956	1000	1,4
# 2X3510.338	900	4
# 2X3515.054	1000	1,4
# 2X3524.541	1000	1,4







Wavelength (angstroms)	Intensity <sup>&amp;</sup>	Region Seen <sup>ç</sup>
# 2X3566.372	2000	4
# 2X3610.462	1000	4
# 2X3619.392	2000	1,4
# 2X3624.733	150	4



## TUNGSTEN I

Wavelength (angstroms)	Intensity <sup>&amp;</sup>	Region Seen <sup>¢</sup>
3508.735	9	1
3545.229	12	1
3551.028	7	1
3554.213	9	1
3570.655	15	1
3606.067	12	1
3617.521	35	1,4
3632.708	9	1
3641.852	7	1
3654.71		1
3682.101	25	1
3707.931	20	1
3757.923	15	1
3760.133	15	1
3768.447	20	1
3773.705	20	1
3780.770	20	1
3809.228	25	1
3817.480	18	1,4
3829.133	12	1
3835.049	15	1,4
3838.504	15	1
3842.303	10	1
3846.214	20	1
3847.501	18	1
3864.336	12	1
3867.986	30	1,4
3872.835	12	1
3881.402	20	1,4
3955.310	12	1
3965.145	12	1
3983.288	12	1



Wavelength (angstroms)	Intensity <sup>&amp;</sup>	Region Seen <sup>ç</sup>
4005.404	8	1
4008.769	45	1,4
4015.216	25	1
4019.231	18	1
4028.790	12	1
4045.601	12	1,4
4047.948	9	1
4069.804	7	1
4070.608	15	1
4074.374	50	1,4
4088.333	12	1
4102.713	35	1
4114.827	7	1
4118.184	9	1
4157.036	3	1
4171.185	25	1
4207.053	25	1
4219.383	25	1
4241.448	30	1
4244.374	40	1,4
4269.392	40	1,4
4294.623	50	1,4
4302.123	60	1,4
4355.165	15	1
4361.815	20	1
4372.528	25	1
4378.493	25	1
4412.199	20	1
4449.010	20	1
4466.729	20	1
4484.189	35	1
4504.857	30	1
4513.300	30	1



Wavelength (angstroms)	Intensity <sup>&amp;</sup>	Region Seen <sup>ç</sup>
4551.850	35	1
4586.846	30	1
4592.422	20	1
4609.915	50	1
4613.316	50	1
4642.564	30	1
4659.867	200	1
4680.520	150	1
4757.549	60	1
4843.828	50	1
4886.912	50	1
4982.603	40	1
5006.157	40	1
5015.321	40	1
5053.296	60	1
5054.608	25	1
5069.146	50	1
5224.667	50	1
# 2X3373.754	10	1
# 2X3457.366	9	1
# 2X3508.735	9	1
# 2X3510.032	10	1
# 2X3545.229	12	1
# 2X3570.655	15	1
# 2X3606.067	12	1
# 2X3617.522	35	1
# 2X3632.708	9	1
# 2X3682.092	25	1
# 2X3707.931	20	1
# 2X3757.923	15	1
# 2X3760.126	15	1
# 2X3768.447	20	1
# 2X3780.770	20	1





Wavelength (angstroms)	Intensity <sup>&amp;</sup>	Region Seen <sup>ç</sup>
# 2X3829.127	12	1
# 2X3842.303	10	1
# 2X3846.214	20	1
# 2X3847.490	18	1
# 2X3864.335	12	1
# 2X3867.975	30	1
# 2X3872.830	12	1
# 2X3881.390	20	1
8017.18	25	1
# 2X4019.231	18	1
# 2X4045.601	12	1
# 2X4069.154	7	1
# 2X4070.606	15	1
# 2X4074.364	50	1
# 2X4102.704	35	1
# 2X4171.185	25	1
# 2X4244.373	40	1
# 2X4269.392	40	1
# 2X4294.614	50	1

\* Transitions into a metastable state

# Seen in second order

ç Regions:

1. Three cm from anode
2. Tube center
3. 19 cm from cathode
4. Five cm from cathode
5. Three cm from cathode

& The intensities listed are relative intensities for each element only and were taken from the following: Argon I from the American Institute of Physics Handbook; Nickel I and Tungsten I from the MIT Wavelength Tables. These intensities agreed reasonably well with the visual estimates.













thesK46

A spectroscopic investigation of an argo



3 2768 002 10886 2

DUDLEY KNOX LIBRARY